Determination of the plastic viscosity of superplasticized cement pastes through capillary viscometers

Ángel de la Rosa [(a)], Elisa Poveda [(a)], Gonzalo Ruiz [(a,*)]
Rodrigo Moreno [(b)], Héctor Cifuentes [(c)] and Lucía Garijo [(a)]

[(a)] ETS de Ingenieros de Caminos, C. y P., Universidad de Castilla–La Mancha,
Av. Camilo José Cela s/n, 13071 Ciudad Real, Spain
[(b)] Instituto de Cerámica y Vidrio (CSIC), Madrid, Spain
C. Kelsen 5, Campus de Cantoblanco, 28049 Madrid, Spain
[(c)] ETS de Ingeniería, Universidad de Sevilla
Camino de los Descubrimientos s/n, 41092 Sevilla, Spain
*Corresponding author: Gonzalo.Ruiz@uclm.es

February 5, 2021

Abstract

Determining the rheological parameters of the cement paste correctly is a matter of capital importance when designing a self–compacting concrete (SCC). For this, it is necessary to resort to rheometers, which are expensive and, therefore, not available in all laboratories. However, the calculation of plastic viscosity can also be carried out using capillary viscometers, simple and cheap instruments whose foundation lies in the time it takes for a volume of suspension to flow through the hole in a capillary. It is common practice to use the Marsh funnel in the construction industry but not the Cannon–Fenske viscometer, more used in other industries such as chemistry. Besides, most of the models associated with the Marsh funnel have been developed for drilling muds, although there are some exclusive for cementitious suspensions. However, the rheological nature of both materials is very similar, so it seems appropriate to check how these models behave in cement pastes designed for SCC. Consequently, the rheological behavior of 39 cement pastes of different composition was studied (varying the nature of cementitious materials and the superplasticizer admixture, with various water–cementitious material ratios) to check the performance of said devices and models using the plastic viscosity measured with a rotational rheometer as a reference. The results indicate that the Cannon–Fenske viscometer offers a better approximation to the reference plastic viscosities than the Marsh funnel. As for the comparison between models for the Marsh funnel, the results obtained are disparate, so it would be convenient to expand the experimental research to adjust the parameters of the models that offer a good approach.

KEYWORDS: superplasticized cement paste, rheology, plastic viscosity, Cannon–Fenske viscometer, Marsh funnel.

NOMENCLATURE

b_i	Coefficient for calculating non–dimensional coefficient of the flux
c_i	Coefficient for calculating non–dimensional coefficient of the flux
CI	Confidence interval
g	Acceleration of gravity
GGBS	Ground–granulated blast–furnace slag
h	Capillary tube length of the Marsh funnel
H	Height of suspension at any time inside the Marsh funnel
H_0	Initial height of suspension inside the Marsh funnel
H_f	Final height of suspension inside the Marsh funnel
k_1	Calibrated coefficient of the first bulb of a Cannon–Fenske viscometer
k_2	Calibrated coefficient of the second bulb of a Cannon–Fenske viscometer
K	Non–dimensional coefficient of the flux
$N_1 = \sigma_{xx} - \sigma_{yy}$	First coefficient of stress tensor
$N_2 = \sigma_{yy} - \sigma_{zz}$	Second coefficient of stress tensor
n'	Flow behavior index
P	Pressure drop along the capillary tube
Q	Flow drainage rate
r	Radius of the capillary tube of viscometer
rpm	Number of revolutions per minute
r_0	Radius of the capillary tube of the Marsh funnel
R	Radius at any height of suspension inside the Marsh funnel
R_0	Radius of initial height of suspension inside the Marsh funnel
R_f	Radius of final height of suspension inside the Marsh funnel
s	Correction coefficient for non–Newtonian fluids
SP/*c*	Superplasticizer / cementitious materials ratio
t_f	Time of drainage for a determinate volume of suspension inside the Marsh funnel
t_0	Constant of time
t_1	Time the suspension takes to flow through the first bulb of the Cannon–Fenske viscometer
t_2	Time the suspension takes to flow through the second bulb of the Cannon–Fenske viscometer
V	Volume of suspension drained out of the viscometer
V_0	Initial volume of suspension inside the Marsh funnel
w/c	Water–cementitious materials ratio
α	Angle between the generatrix and the longitudinal axis of the Mars funnel
$\dot{\gamma}$	Shear rate
$\dot{\gamma}_w$	Wall shear rate
η	Plastic viscosity
η_e	Effective viscosity
η_p	Plastic viscosity of cement paste
η_w	Plastic viscosity of water
$[\eta]$	Intrinsic viscosity

ν	Kinematic viscosity
ρ	Density
ρ_c	Cementitious materials density
ρ_p	Cement paste density
ρ_{SP}	Superplasticizer density
ρ_w	Water density
σ_{ij}	Component of stress tensor
τ	Shear stress
τ_w	Wall shear stress
τ_0	Yield stress
ϕ_c	Volume fraction of cementitious materials
ϕ_m	Maximum packing density

1 Introduction

The rheological behavior of cement pastes is an issue on which there is abundant technical literature [1–33]. These suspensions exhibit a flow curve (constitutive relationship between shear stress, τ, and shear rate, $\dot{\gamma}$) that responds to the rheological model of Herschel–Bulkley [5, 25, 29, 30]. These parameters do not have a fixed value but depend on multiple factors, mainly associated with the colloidal nature of cementitious particles (characterized by their tendency to cluster) and the interactions produced between them and with the polymer chains of the superplasticizer admixture that is added to the suspension [27, 31]. In particular, η varies according to the nature of particles, their morphology, and their size distribution. It also depends on the geometry and the characteristics of the rheometer on the testing procedure [34, 35] and on conditions like pressure, temperature, etc [35]. Thus, a cementitious suspension can show a flow curve with different stretches [5] in which the value of the slope (plastic viscosity of the cement paste, η_p) can decrease (shear thinning [11]), increase (shear thickening [7, 13]) or remain constant (linear behavior). Another interesting feature of these systems, inherent to their colloidal nature, is the evolution they experience over time, which manifests with the formation of a hysteresis loop in the flow curve, a phenomenon known as thixotropy [2, 3, 14, 36]. However, when the pastes are completely deflocculated, the Bingham model can be used as an approximation of their rheological behavior, which is described using two main rheological parameters: yield stress, τ_0, and plastic viscosity η_p [31, 37].

The knowledge of rheological behavior of cementitious materials is fundamental in new applications of concrete [34]. Digital fabrication technologies, such as 3D printing processes, requires to study the rheological properties of the material [38–40]. Casting processes, such as pumping, involves the creation of a lubrication layer on the pipe wall, the rheological properties of which are fundamental for the correct execution [41, 42]. Particularly interesting are mix design methods for self–compacting concrete based on rheological criteria [43], such as the one recently proposed by some of the authors of this article for self–compacting steel–fiber reinforce concrete [44], which requires to know the value of η_p as a starting point. This parameter can be easily measured using a rheometer; but rheometers are complex and expensive, and thus they are not available to all users. Besides, they are not compatible with all field applications [37]. This fact highlights the possibility of using, as an alternative, other instruments that are more affordable and, at the same time, allow us to obtain good approximations to the actual rheological properties [37]. This is the case of capillary viscometers, which are frequently used by different industries, both in field and laboratory work, due to their simplicity, ease of use, and low cost. The Cannon–Fenske viscometer and the Marsh funnel stand out within this typology of viscometers.

The Cannon–Fenske viscometer appears in 1938 to measure kinematic viscosity values, ν, in petroleum-derived materials [45, 46]. This viscometer has been used primarily in the chemical industry [47–49], and within the scope of the chemistry of cementitious suspensions, it has been used to measure values of ν and η, both in admixtures [50] and in their dispersant fluids [28].

The Marsh funnel [51–53] arises almost at the same time as the Cannon–Fenske viscometer (1931), and, since then, its use has been continuous in the oil well drilling and gas extraction industries, as well as in mining and construction. Its characteristics vary according to the application, but the basis is the same in all cases. Some works have tried to establish, both analytically and numerically, expressions that allow the calculation of the main rheological parameters in Newtonian and non–Newtonian suspensions [52–61]. Le Roy and Roussel [16, 32] deduced a series of analytical equations for cementitious suspensions that allow the calculation of the rheological parameters assuming the hypothesis of non–Newtonian linear Bingham behavior. Ferrara *et al.* [37] studied the rheological behavior of cement pastes for self–compacting concrete using the expressions developed by Roussel *et al.* [16]. D′Aloia *et al.* [62] estimated the optimal dose of superplasticizer admixture to be used in self–compacting concrete cement pastes. Also noteworthy are the works of Nguyen *et al.* [63] in cement slurries, Jayasree *et al.* [21] in cement pastes, Schoesser *et al.* [64] in bentonite sludges. Finally, as regards numerical investigations, it is worth mentioning the work of Cremonesi *et al.* [37, 53, 65], where the material inside the funnel is simulated by finite elements and that of Balhoff *et al.* [66] that present a method based on the Runge–Kutta technique for the calculation of rheological parameters.

This study arises as a result of the development of a new design methodology for self–compacting steel–fiber reinforced concrete [44] and the need to measure the value of the plastic viscosity of the cement paste. According to the background of Ferrara *et al.* [37], in which the measurements obtained with a rotational rheometer and the Marsh funnel are compared, the inclusion of the Cannon–Fenske viscometer is proposed as a new measuring device. For this purpose, an extensive experimental campaign has been carried out with a total of 39 cement pastes of different compositions. The objectives pursued are, first of all, to verify whether it is possible to determine η_p by the Cannon–Fenske viscometer. As far as we know, there are no publications that deal exclusively with the experimental measurement of η_p of cement pastes with this device. Only one preliminary reference was found in cement slurries using a capillary tube (one meter high and 3.3 mm in diameter) [67]. However, the dimensions of this device do not make it suitable for field use. Secondly, compare these results, together with those obtained through the Marsh funnel, with the measurements of a rotational rheometer, in the same cement pastes, and with the η_p predictions based on the paste composition made by the equation of Krieger and Dougherty [33, 68]. Finally, it is intended to analyze the η_p results calculated through the application of different models associated with the Marsh funnel existing in the specialized literature.

2 Models for calculating plastic viscosity using capillary viscometers

2.1 Starting hypotheses

To apply the different calculation models, it is necessary to establish a series of starting hypotheses:

- The suspensions are completely deflocculated, and their behavior can be described using the Bingham model (with a constant value of η_p over a wide range of $\dot{\gamma}$ and τ_0 next to zero).
- The flow is fully developed and has the following properties: it is quasi–stationary, isothermal, incompressible, one–dimensional, the regime is laminar, and there is no sliding on the walls of the viscometer.

- The volume inside the funnel varies slowly over time, especially at the end of the test [53, 55, 66], and the speed of the suspension at the exit orifice is a function of its level within the instrument [16, 32, 53, 55, 66].

2.2 Physical fundamentals of capillary viscometers

Both the Cannon–Fenske and the Marsh funnel belong to the typology of viscometers operating under pressure flow [35]. They consist of a tank, connected to a capillary, in which a suspension is introduced and on which pressure is generated by the effect of gravity, producing the flow of the sample through the outlet orifice. These devices can only measure stationary shear functions, that is, η and the normal stress coefficients of the stress tensor of the material N_1 ($N_1 = \sigma_{xx} - \sigma_{yy}$) and N_2 ($N_2 = \sigma_{yy} - \sigma_{zz}$) oriented in the direction of flow (x, y, and z are the directions of the flow) [35]. Both $\dot{\gamma}$ and τ vary linearly from a maximum in the wall (where the flow velocity is equal to zero) to be annulled on the capillary axis (maximum flow velocity) [35]. Thus, in a Newtonian fluid, it is fulfilled:

$$\dot{\gamma}_w = \frac{4\,Q}{P\,r_0^3} \tag{1}$$

$$\tau_w = \frac{P\,r_0}{2\,h} \tag{2}$$

$$\eta = \frac{\tau_w}{\dot{\gamma}} \tag{3}$$

In these expressions, τ_w is independent of the rheology of the sample, but $\dot{\gamma}_w$ depends on its rheological behavior and must be corrected by a factor s in the case of non–Newtonian fluids [35]:

$$\dot{\gamma} = \frac{\dot{\gamma}_w(3+s)}{4} \tag{4}$$

$$s = \frac{d\dot{\gamma}_w}{d\tau_w} \tag{5}$$

The flow time measured by these viscometers is associated with the characteristics of the apparatus and can be related to the rheological parameters in both Newtonian and non–Newtonian linear behavior materials (those that follow the Bingham model), where the value of η is constant along the curve $\tau - \dot{\gamma}$ and the value of τ_0 is close to zero [16, 32]. This hypothesis is adopted in this paper for the study of cement pastes with superplasticizer admixture.

Whether the Cannon–Fenske viscometer or Marsh funnel is used, it is essential to select the appropriate capillary diameter of the instrument so that the solid particles in the suspension do not clog up the orifice, especially in the case of the Cannon–Fenske viscometer. According to Le Roy and Roussel [16, 32], Marsh funnel has two limitations: if the value of η_p is very low there is no linear relationship with t_f and, therefore, this value is not a significant measure from a rheological point of view. On the other hand, the pressure gradient generated by the weight of the suspension must be sufficient so that the value of τ_w in the capillary wall is greater than τ_0, and flow can occur. This aspect has been studied in the case of cement pastes by Le Roy and Roussel [16, 32].

2.3 Marsh funnel

Several models calculate the value of η from the measurement of the different levels of a sample volume within the funnel at the beginning, during and at the end of the test, together with the geometric parameters of the apparatus and t_f, which is the time it takes to drain said sample volume. The most important ones available in the technical literature are described below.

2.3.1 *Model of Le Roy and Roussel*

The model of Le Roy and Roussel [16, 32] allows to relate t_f in cementitious suspensions of Bingham–type rheological behavior with the value of η_p. This approach depends on the geometric characteristics of the instrument and requires a low value of τ_0 of the material, which holds true in cement pastes with superplasticizer admixture. From measurements of different levels of the suspension inside the funnel before and after a certain volume of material drains through the capillary, the model provides the value of η_p from the following two equations:

$$H = \frac{1}{\tan\alpha}\left[\left(\left(H_0\tan\alpha + r\right)^3 - \frac{3}{\pi}V\tan\alpha\right)^{\frac{1}{3}} - r\right] \tag{6}$$

$$\begin{aligned} t_f = &\frac{8\,\eta_p}{3\,\rho_p\,g\,r^3\,\tan\alpha}\left\{\left(1+\frac{3h}{r}\tan\alpha\right)\left[\frac{1}{2}\left(H_0-H\right)\left(H_0+H+2h\right)\tan^2\alpha - \right.\right. \\ &- 2\left(h\tan\alpha - r\right)\left(H_0-H\right)\tan\alpha + \left(h\tan\alpha - r\right)^2\,\ln\frac{H_0+h}{H+h}\left.\right] - \\ &\left. - \frac{r^3}{h\tan\alpha - r}\left[\ln\frac{H_0\tan\alpha + r}{H\tan\alpha + r} - \ln\frac{H_0+h}{H+h}\right]\right\} \end{aligned} \tag{7}$$

where ρ_p is the density of the paste, g is the acceleration of gravity, and the meaning of the geometrical parameters can be checked in Fig. 3.

The procedure to use Eqs. 6 and 7 is as follows. A certain amount of suspension is introduced into the funnel, which can vary between $0.8\,\mathrm{dm}^3$ and $1.7\,\mathrm{dm}^3$, according to the authors and the country's standards, such as ASTM C939–94a, EN 445 or EN12715. We selected $0.8\ \mathrm{dm}^3$ as the initial quantity; once introduced in the funnel, we write down the height as H_0. Then we open the hole and start measuring the time it takes a fraction of the initial amount to flow, which is $0.4\,\mathrm{dm}^3$ if $0.8\,\mathrm{dm}^3$ is used as the initial amount, or $1\,\mathrm{dm}^3$ if $1.7\,\mathrm{dm}^3$ is used as the initial content. Once $0.4\,\mathrm{dm}^3$ are drained, close the hole and write down the value of the final height, H_f. The time it takes to drain $0.4\,\mathrm{dm}^3$ is t_f. H (Eq. 6) is a parameter that only depends on the initial height measured in the funnel before draining the suspension and the volume drained in the test during the time t_f (in our case $0.4\,\mathrm{dm}^3$). It may happen that the suspension does not drain, that is, it has a yield stress value so high that the suspension cannot leave the funnel: in this case, $H = H_0$; if the total introduced volume ($0.8\,\mathrm{dm}^3$) is allowed to drain, then H is equal to 0. Actually, H is an auxiliary parameter that, depending on the volume of suspension introduced and the volume of suspension drained, allows to go to Eq. 7 to calculate the plastic viscosity value of the suspension, once the time it took to flow $0.4\,\mathrm{dm}^3$ (t_f) and the density of the suspension is measured. Therefore, first, we must calculate H from the initial measurement of H_0 and the volume V drained. Then we have all the data to get into Eq. 7 (H, H_0, ρ_p, t_f, capillary height h, capillary radius r and angle of the generatrix α).

2.3.2 *Model of Guria et al.*

The model of Guria *et al.* [55] allows us to establish the relationship between τ_w and $\dot{\gamma}_w$ on the Marsh funnel wall and, from it, calculate η. To do this, first of all, you have to estimate the value of τ_w with Eq. (8):

$$\tau_w = \frac{\rho g\left(H+h\right)}{\frac{H}{\left[r+(R_0-r)(H/H_0)\right]\cos\alpha} + \frac{2h}{r}} \tag{8}$$

In the common area between the conical and cylindrical parts of the apparatus, Eq. (8) is simplified in

Eq. (9):

$$\tau_w = \frac{1}{2}\rho g r \tag{9}$$

The level of the suspension inside the Marsh funnel, H, can be calculated by knowing the geometry of the apparatus and the discharge volume, V:

$$H = \sqrt[3]{\frac{V_0 - V - \pi r^2 h}{(\pi/3)\,(R_0/H_0)^2}} \tag{10}$$

In this model, the value of $\dot{\gamma}_w$ is determined with Eq. (11), deduced from Brydson [53, 69]:

$$-\dot{\gamma}_w = \frac{3\,n' + 1}{4\,n'}\,\frac{4\,Q}{\pi r^3} \tag{11}$$

The discharge rate, Q, is calculated with the slope of the drained volume–time curve, $V - t_f$. In Eq. (11), n' is the flow behavior index, which can be estimated with the following equation:

$$n' = \frac{\mathrm{d}\log\tau_w}{\mathrm{d}\log\left(4Q/\pi r^3\right)} \tag{12}$$

where d stands for derivative. Using these expressions you can draw the consistency diagram, which corresponds to the discharge flow curve of the suspension, as it relates τ_w and $\dot{\gamma}_w$. When assuming the hypothesis of Bingham rheological behavior, the value of the slope of the $\tau_w - \dot{\gamma}_w$ curve, within the range of $\dot{\gamma}_w$ in which the viscometer works, is the value of η [55].

2.3.3 *Model of Balhoff et al.*

Like Guria *et al.* [55], Balhoff *et al.* [66] derive an expression from calculating τ_w in non–Newtonian fluids from the level of the suspension that remains inside the funnel during drainage, H:

$$\tau_w = \frac{\rho g(H + h)}{\frac{2H_0}{R_0} + \frac{2h}{r}} \tag{13}$$

To apply this model, the $\tau_w - \dot{\gamma}_w$ curve is also represented assuming the same rheological behavior as in the model of Guria *et al.* [55]. The values of H and $\dot{\gamma}_w$ are calculated with Eqs. (10), (11) and (12) of the model of Guria *et al.* [55].

2.3.4 *Model of Sedaghat*

Sedaghat [53] develops a model similar to that of Guria *et al.* [55], which allows obtaining the values of τ_w and $\dot{\gamma}_w$ on the Marsh funnel wall. In this case, the energy loss is calculated using Bernoulli's equation through the discharge rate Q [53, 60]:

$$Q = \pi r^2 K \sqrt[2]{2gH} \tag{14}$$

The dimensionless flow coefficient, K, is calculated with the values of t_f and H, for complete drainage of the suspension, using Eq. (15) proposed by Sedaghat *et al.* [53, 60]:

$$t_f = \begin{cases} (b_1 + b_2 H^{1/2} + b_3 H^{3/2} + b_4 H^{5/2})/K & \text{if} \quad H \geq h \\ (c_1 + c_2 H^{1/2})/K & \text{if} \quad H < h \end{cases} \tag{15}$$

K is a function that depends on the flow properties of the suspension. The b_i and c_i coefficients of this analytical solution can be calibrated and adjusted to the characteristics of the material through the $H - t_f$ curves [53]. However, for the sake of simplicity, K is considered constant, and the b_i and c_i coefficients proposed by the author (see Table1) are only for a standard Marsh funnel [53, 70, 71] and a discharge volume of $1500\,\mathrm{cm}^3$.

b_1	$38.6093038\ \mathrm{cm}^{1/2}$
b_2	-0.778
b_3	$0.127\ \mathrm{cm}^{-1}$
b_4	$-0.00929\ \mathrm{cm}^{-2}$
c_1	$0.10176826\ \mathrm{cm}^{1/2}$
c_2	-0.0452

Table 1: Coefficients of the model proposed by Sedaghat [53].

The following equation relates τ_w and K [53]:

$$\tau_w = \frac{1}{2}\rho g H \left(1 - K^2\right) \frac{r}{h} \tag{16}$$

Sedaghat suggests a modification of Eq. (11) of the model of Guria *et al.* [55] to take into account the entire geometry of the Marsh funnel and not just the section of the outlet capillary [53]. Thus, for non–Newtonian fluids, the following equation is formulated:

$$-\dot{\gamma}_w = \frac{(3n' + 1)\, QH}{2\pi\, n' r^3 h} \tag{17}$$

2.3.5 *Model of Pitt*

Pitt [52] conducts a numerical study of the flow through the Marsh funnel for non–Newtonian suspensions and establishes the following equation, that links t_f with η:

$$\eta_p = \exp\left[\frac{\ln\left(\frac{t_f - t_0}{0.58}\right)}{1.2} + \ln\rho\right] \tag{18}$$

which can be simplified as:

$$\eta_p = 1.57\rho\left(t_f - t_0\right)^{0.83} \tag{19}$$

These equations depend on the density of the material, ρ, and a constant, t_0, set according to the volume to be tested ($t_0 = 26\,\mathrm{s}$, if performed with $1\,\mathrm{dm}^3$ of suspension, or $t_0 = 24.5\,\mathrm{s}$, if a volume equal to $0.946\,\mathrm{dm}^3$ is drained). The coefficients of the equations correspond to the centimeter–gram–second system of units, that is, density ρ should be introduced in g/cm^3 and time t_f in seconds, whereas the plastic viscosity is obtained in centipoises [cP], which are equivalent to mPa s.

3 Materials and methodology

3.1 Materials

The composition of the cement pastes to be studied was carried out based on the following criteria: use a common cement (CEM II 32.5 BL–II) and another with a high content of Portland clinker (CEM I 52.5–SR); use an active mineral addition as a replacement for part of the cement (ground granulated blast–furnace

slag, GGBS); prepare cement pastes that serve as a basis for the design of self–compacting concrete by using superplasticizer admixtures of different characteristics. Prior to the selection of these design criteria, the work of Puertas *et al.* [72] and Alonso *et al.* [73] in which the effect of different superplasticizer admixtures on rheological properties in cement pastes with different chemical and mineralogical composition was accounted for.

Two types of Portland cement (CEM I 52.5–SR and CEM II 32.5 BL–II) and GGBS as a mineral addition have been used to make the pastes. The superplasticizers used are of the type of modified polycarboxylates in aqueous base (Sika ViscoCrete–20 HE, ρ_{SP} = 1090 kg/m^3 and dry residue of 40%) and poly–aryl–ether (BASF MasterEase–5025, ρ_{SP} = 1058 kg/m^3 and 30% dry residue). The experimental design of cement pastes is specified below:

- 31 cement pastes made with four types of cementitious materials, namely CEM I 52.5–SR, CEM II 32.5 BL–II, 75% CEM I 52.5–SR and 25% GGBS, 75% CEM II 32.5 BL–II and 25% GGBS; each type was made with the following water / cementitious materials ratios, w/c: 0.35, 0.47, 0.53, 0.63; and with two amounts of superplasticizer admixture (Sika ViscoCrete–20 HE) in relation to cementitious materials, *SP*/c, 0.4 and 0.8%.

- 8 cement pastes made with CEM I 52.5–SR and, again, using various w/c ratios, 0.40, 0.47, 0.53 and 0.63, and two *SP*/c ratios (BASF MasterEase–5025), 1.0 and 1.2%.

The particle size distribution of the cementitious materials (Fig. 1) was obtained by laser diffraction granulometry using an optical system Mastersizer 2000).

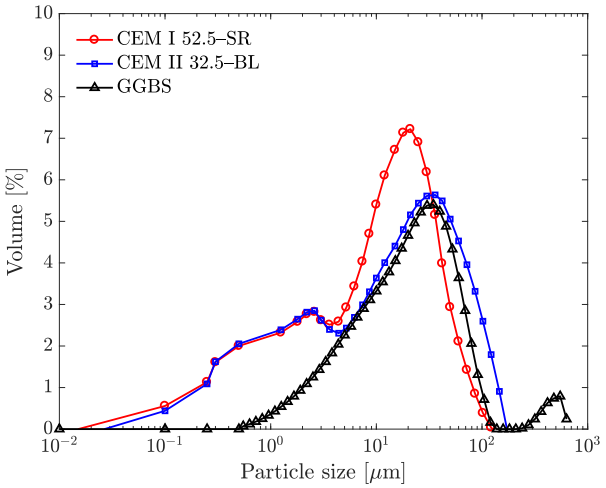

Figure 1: Particle size distribution of cementitious materials.

3.2 Mixing protocol

Cement pastes were manufactured with a Kitchen–Aid mixer with a capacity of 4.8 dm^3. The mixing sequence was as follows: first, cementitious materials and 90% of the water are added, remaining for 30 seconds at rest. Next, a shaft rotation speed of 64 revolutions per minute, rpm, is selected for 60 s. After this time, the mixing is stopped, the adhered material is scraped to the edges of the container and the blades, and the superplasticizer

admixture is mixed together with the rest of the water (90%). Mix again for 90 s at a speed of 92 rpm, and the process is finished. The mixing protocol was established based on the recommendations of ASTM C305–99 and AASHTO T162–04 [74, 75].

3.3 Rheometric tests

The plastic viscosity of the cement pastes were measured with three instruments: a rotational rheometer, a Cannon–Fenske viscometer and a Marsh funnel (see Fig. 2). The rotational rheometer, with double cone–plate sensor (Haake RS50), serves as a reference for measurements.

Figure 2: Measuring instruments: Haake RS50 rotational rheometer (left), Cannon–Fenske viscometer (center) and Marsh funnel (right).

3.3.1 *Rotational rheometer*

The tests performed with the Haake RS50 rotational rheometer were carried out under shear rate control and preventing slippage between the suspension and the walls of the double cone–plate sensor of the instrument, which exerts a uniform shear rate throughout the sample. Each test was carried out at a constant temperature of 25 °C. The samples were introduced into the rheometer and a first measurement was made following this rheological protocol: an ascending ramp from 0 to 600 s^{-1} during 180 s; a constant strain rate equal to 600 s^{-1} during 120 s; a descending ramp from 600 to 0 s^{-1} during 180 s. This protocol is similar to the ones used in [27, 37, 62, 76, 77] to obtain steady flow properties [34]. The first test is a pre–shear one in order to break down the structure and homogenize the sample. Then, 60 s were waited and the measurement was repeated with the same protocol. Again, after 60 s the rheometric test was repeated. Figure 4 shows the resulting flow curves for the paste made with CEM I 52.5-SR only, w/c = 0.63, *SP*/c = 0.8. The use of the flow curve approaches better to the behavior measured with the other techniques in which samples are measured during flow conditions. The use of stationary measurements is not desired in complex particulate suspensions since, at every step, the paste could exhibit high apparent yield stress that results in torque overloading. The flow

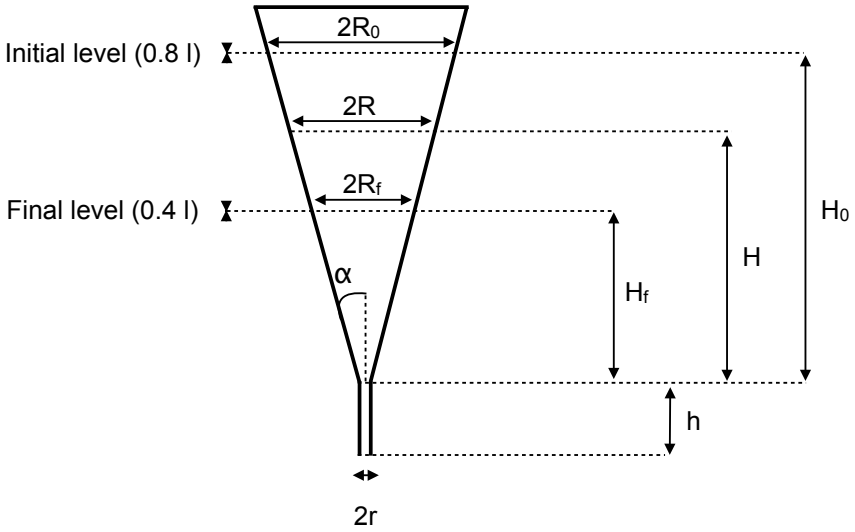

Figure 3: Marsh funnel geometry.

curve is considered to be that formed by the pairs of points $\tau - \dot{\gamma}$ of the downward branch of the second and third tests. It is used to calculate the plastic viscosity of the material tested according to the adjustment of data to the Bingham model. It should be noted that this research only seeks to find the values of plastic viscosity, but not the yield stress values. In that case, a different test protocol would be more convenient since yield stress must be determined at a very low shear rate in a steady state of the flow (in stress control and by steps of a certain duration) [35].

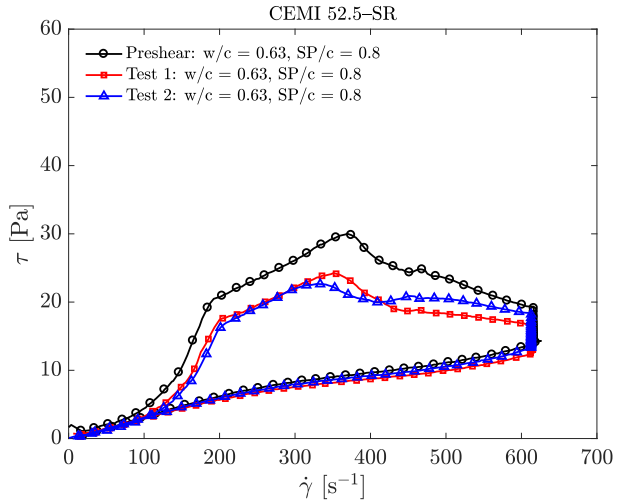

Figure 4: Curves resulting from applying the test protocol three times.

3.3.2 *Cannon–Fenske viscometer*

The test with the Cannon–Fenske viscometer is performed according to the specifications of ASTM D445–17a [78]. From the density of the suspension, ρ, the plastic viscosity of the material, η, is determined according

to the temperature conditions of the sample during the test with Eqs.(21) and (20):

$$\eta = \nu\,\rho, \text{ where} \tag{20}$$

$$\nu = \frac{k_1\,t_1 + k_2\,t_2}{2} \tag{21}$$

where t_1 and t_2 are the efflux time that the suspension takes to go through the first and second bulb of the viscometer, respectively, and k_1 and k_2 are calibrated constants.

The Cannon–Fenske viscometer is used with opaque fluids and consists of two bulbs, so that two measurements of ν and η_p are performed in a single test. It is important to select previously the diameter of the capillary, which should allow the flow and avoid clogging by accumulation of solid particles of the suspension. Also, the capillary must not be too wide to prevent the flow from being too fast, which results in inaccurate measurements (the latter aspect was checked using a Cannon–Fenske 300 series viscometer, with a capillary diameter equal to 1.26 mm). The diameter of the capillary selected in this study is equal to 1.88 mm (Cannon–Fenske 400 series; see Fig. 2). The value of the constants certified by the calibration laboratory for each bulb are as follows:

- bulb 1: k_1 = 1.10630 mm^2/s^2 and 1.11070 mm^2/s^2, for 40°C and 100°C, respectively,
- bulb 2: k_2 = 0.84243 mm^2/s^2 and 0.84574 mm^2/s^2, for 40°C and 100°C, respectively.

By having two reference points calibrated in each bulb, the value of the constants k_1 and k_2 can be calculated for the temperature of the cement paste during the test. The test is carried out in accordance with ASTM–D445–17a [78] and the procedure is as follows: the fluid to be tested is introduced at one end of the instrument by aspiration with a pipette until a small reservoir is filled and then, the time it takes for the flow to pass through two marks in two consecutive bulbs is measured.

3.3.3 *Marsh funnel*

The execution of the Marsh funnel test is described in standards EN–445, ASTM–C939M–16a, and UNE–EN–12715 [79–81]. The procedure consists of fixing the funnel vertically by the handle and closing the exit hole. A quantity of the sample to be tested is then introduced (0.8 dm^3 is established as the initial volume), and then the filling height in the conical part of the funnel, H_0, is measured. Then the hole is opened, and the time t_f taking to drain 0.4 dm^3 of suspension is measured. At the exit of the hole, a graduated beaker is placed in which the drained suspension is collected. To conclude the test, the hole is closed and the height of the fluid inside the funnel, H_f, is recorded again. The drainage time, t_f, depends on the physical properties of the material and the geometry of the funnel (Fig. 3), one of the most influential parameters being the radius of the outlet capillary, r, whose value is 2.3 mm in our case. As for this last parameter, it is important to properly select the capillary diameter, for the same reasons described above for the Cannon–Fenske viscometer. The tests done with the Marsh funnel have been recorded with a digital camera, being able to determine a sufficient number of points to draw the consistency curve, $\tau_w - \dot{\gamma}_w$, of the suspensions.

3.3.4 *Density measurement*

The value of ρ_p is calculated following the procedure described in UNE–EN–1015-6 [82]. For this, a standardized cylindrical container is used, filling it with a sample and weighing it on a precision balance. The difference between the mass of the filled container of the sample and its empty mass is divided by the volume of the cylinder, determining the value of ρ_p.

4 Results and discussion

Individual measurements of all the parameters to calculate η_p obtained with the different instruments used in this study can be seen in the Data Annex.

4.1 Comparison of measurements made with different instruments

The complete flow behavior of the CEM I 52.5–SR cement paste measured with the rotational rheometer is plotted in Fig. 5 in which it can be seen the existence of a complex flow behavior with a robust thixotropic hysteresis. The plots shown below illustrate the flow just in the descendent ramp where a homogeneous flow regime is achieved similar to that of the viscosimeters. Similar trends are found in the other compositions. Only the descendent ramp of the flow curves are shown for the sake of simplicity. As can be seen in Fig. 5 and 6, the descent branches of the flow curves obtained for the tested materials with the rotational rheometer approximate a Bingham type linear rheological model, described by the following equation:

$$\tau = \tau_0 + \eta\dot{\gamma} \tag{22}$$

The slope of the adjusting straight line to the descending branch of the flow curve is η_p, which value has been calculated in the range 10–100 s^{-1} (Fig. 5). However, to make correct measurements in this range of application (typical in cement pastes for fluid concrete applications), when preparing the samples it is necessary to subject them to a higher shear rate to obtain a homogeneous and completely deflocculated mixture. Hence, the sample preparation shear rate range reaches values of 600 s^{-1}.

As the tests are performed under shear rate control, the points of the flow curve obtained at very low shear rate are not representative to obtain τ_0 [35].

In each suspension, it can be seen that, as w/c and *SP*/c increase, the value of η_p decreases. Table 3 shows the range of plastic viscosity values measured by each instrument in each of the cementitious suspensions, which are close to each other. This is a consequence of the lower concentration of solid particles present in the system and the deflocculating and dispersing effect produced by the added superplasticizer admixture (electrostatic repulsion effect and/or steric hindrance, depending on the nature of the admixture [27, 31, 35]). Besides, the flow curves of the suspensions show thixotropy due to the nature of the cementitious materials. In those curves, ascending branches indicate shear thinning behavior, while descending branches (after shearing) adjust a linear Bingham model. Thus, this plastic viscosity value (slope of descending branches) can be compared to the measures obtained with capillary viscometers, i.e., Cannon–Fenske viscometer and Marsh funnel.

Figures 7 and 8 compare the η_p values measured with the rotational rheometer and those calculated with the Cannon–Fenske viscometer and the Marsh funnel for each suspension. The adjustment of the rotational rheometer measurements of η_p and volume fraction of solid particles, ϕ_c, to the Krieger and Dougherty equation (Eq.23) [33, 68] is also shown. Using MATLAB [83], values of the maximum packing fraction, ϕ_m, and the intrinsic viscosity, $[\eta]$ are calculated. Table 2 includes the calculated values of those parameters. Table 3 summarizes the set of the plastic viscosity results calculated through each instrument.

$$\eta_p = \eta_w \left(1 - \frac{\phi_c}{\phi_m}\right)^{-[\eta]\,\phi_m} \tag{23}$$

Four w/c ratios are represented, equivalent to four–volume fractions of cementitious material, ϕ_c, Eq. (24) [27], and two *SP*/c amounts of polycarboxylate based superplasticizer. The model selected for the Marsh funnel is the one proposed by Le Roy and Roussel since it has been applied and validated in concrete cement paste

investigations [16, 32].

$$\phi_c = \frac{\rho_w/\rho_c}{w/c + \rho_w/\rho_c} \tag{24}$$

In all cases, it is observed that the Cannon–Fenske viscometer offers values of η_p closer to those measured with the rotational rheometer through the Krieger and Dougherty equation. The Marsh funnel shows a better approximation only in the paste composed of CEM I 52.5–SR for ϕ_c values equal to 0.404 and 0.477 and an *SP*/*c* ratio equal to 0.4. This exception is probably due to the fact that, occasionally, the capillary of the Cannon–Fenske viscometer can be reduced in diameter due to the presence of undrained cement particles during the previous washing, and not to a phenomenon related to the rheology of the paste and to the instrument, since the trend of the measurements shows a better approximation of the Cannon–Fenske viscometer. It should also be noted that the Marsh funnel, in general, greatly overestimates the value of η_p with respect to the other two instruments in all paste compositions, for *SP*/*c* equal to 0.4 and 0.8. In addition, as ϕ_c increases (or w/c decreases), the difference between the η_p values measured by the rotational rheometer and those calculated with the Cannon–Fenske viscometer with respect to those achieved with the Marsh funnel significantly increases.

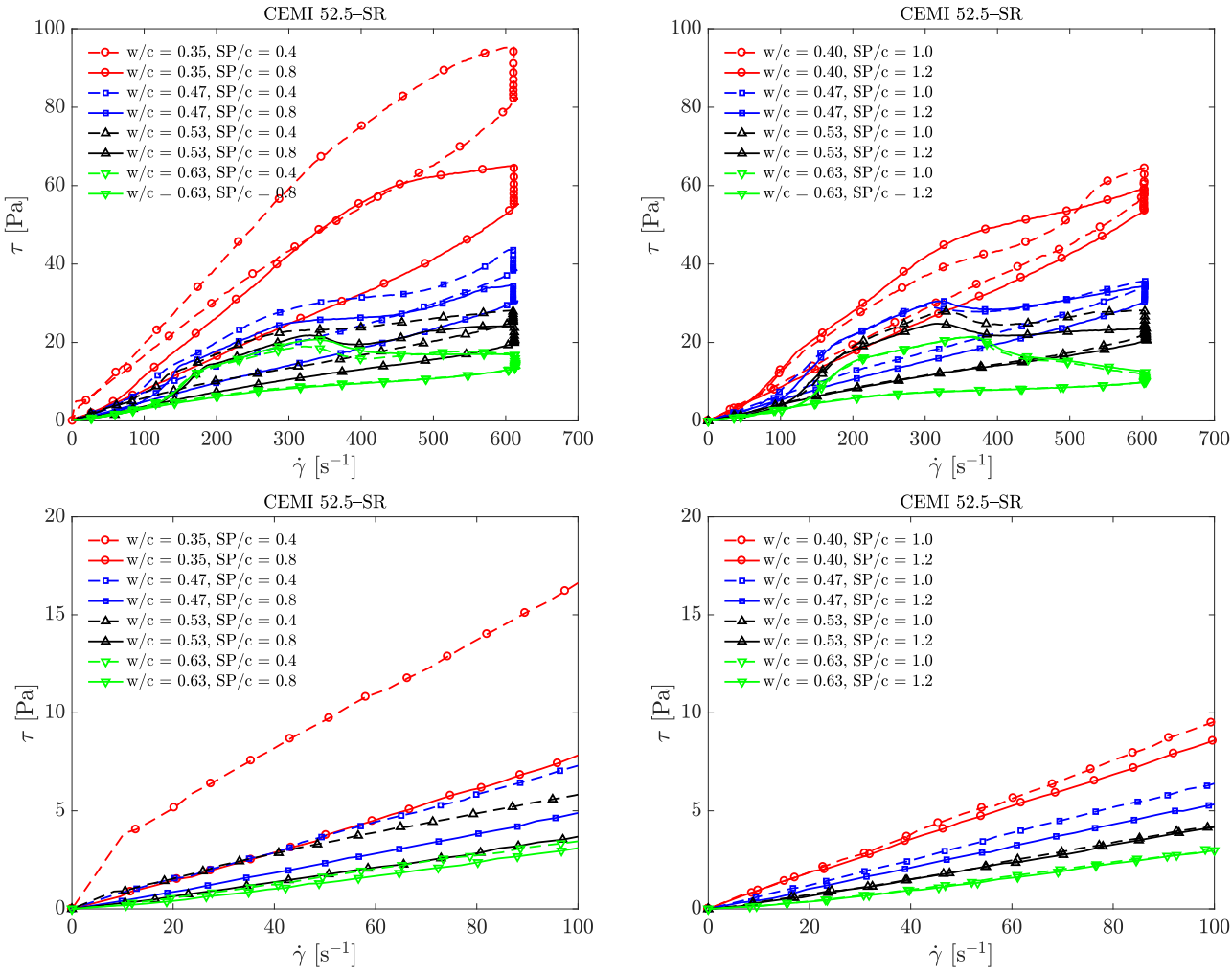

Figure 5: Flow curves obtained with the rotational rheometer for CEM I 52.5–SR cement paste: complete flow curves (upper) and descending branches in the range 0–100 s^{-1} (lower).

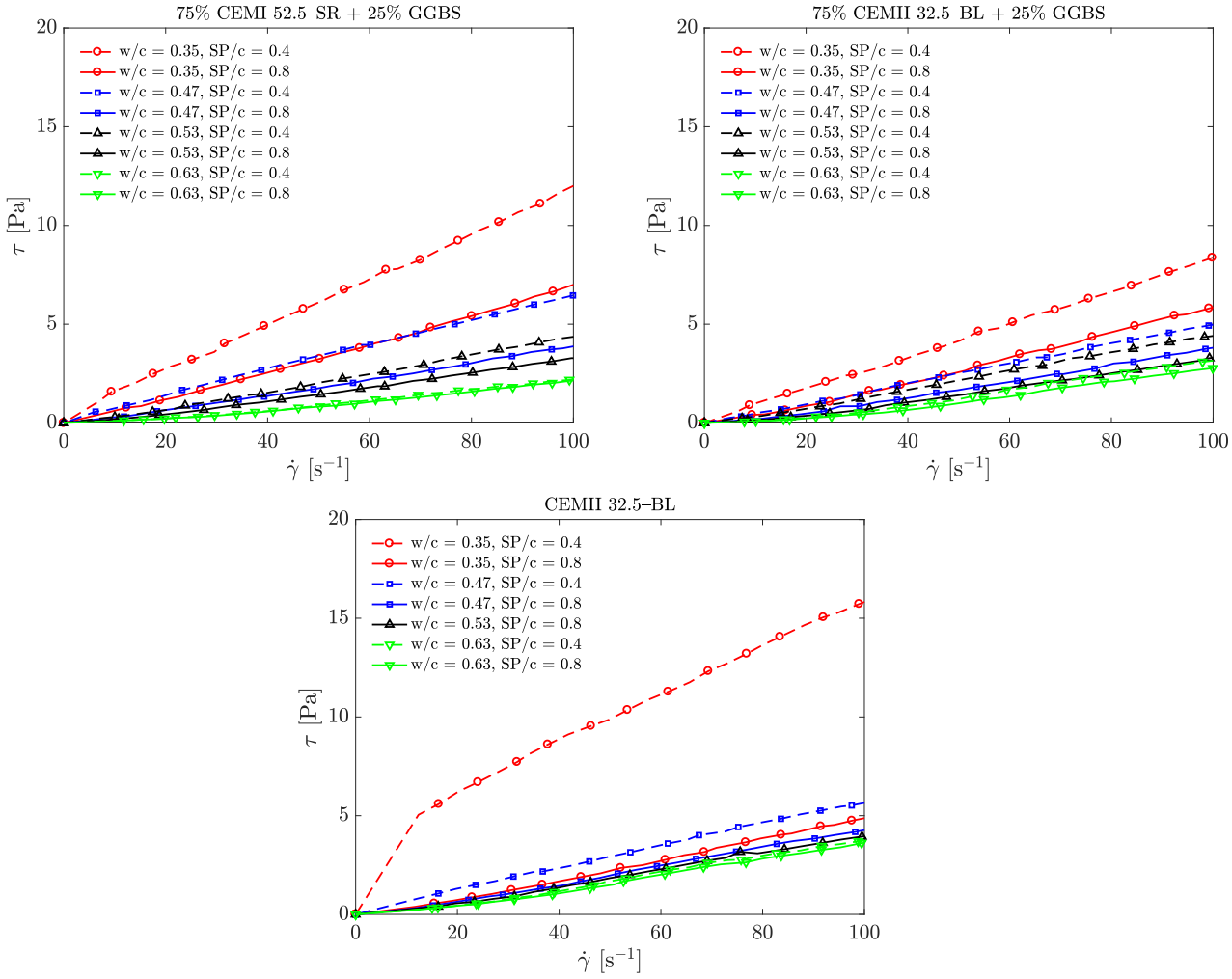

Figure 6: Descending branches of the flow curves obtained with the rotational rheometer for the rest of cement pastes obtained in the range 0–100 s^{-1}.

4.2 Comparison between Marsh funnel models

The Marsh funnel study was carried out on cement suspensions composed only of CEM I 52.5–SR, for four *SP*/*c* ratios, 0.4, 0.8, 1.0 and 1.2 (the first two correspond to the polycarboxylate type superplasticizer admixture modified in aqueous base and the last two to the poly–aryl–ether type). Figure 9 represents the η_p values measured with the rotational rheometer and those calculated from the five models described in this investigation for the Marsh funnel: Le Roy and Roussel model (Eqs. 6 and 7) [16, 32], model by Guria *et al.*(Eqs. 8–12) [55], model by Balhoff *et al.* (Eqs. 10–13) [66], Sedaghat model (Eqs. 14–17) [53] and Pitt model (Eq. 18) [52]. The equation of Krieger and Dougherty [68] is also represented in Fig. 9, with their parameters adjusted to the measurements made with the rotational rheometer. A dispersion of the results offered by each model regarding this equation is observed. For the four *SP*/*c* admixture ratios, the Le Roy and Roussel model gives η_p values higher than those of the Krieger and Dougherty equation, while the Sedaghat and Pitt models show much lower results. The models of Guria *et al.*, and Balhoff *et al.* better approximate the equation of Krieger and Dougherty, presenting values below it in pastes with amounts of superplasticizer

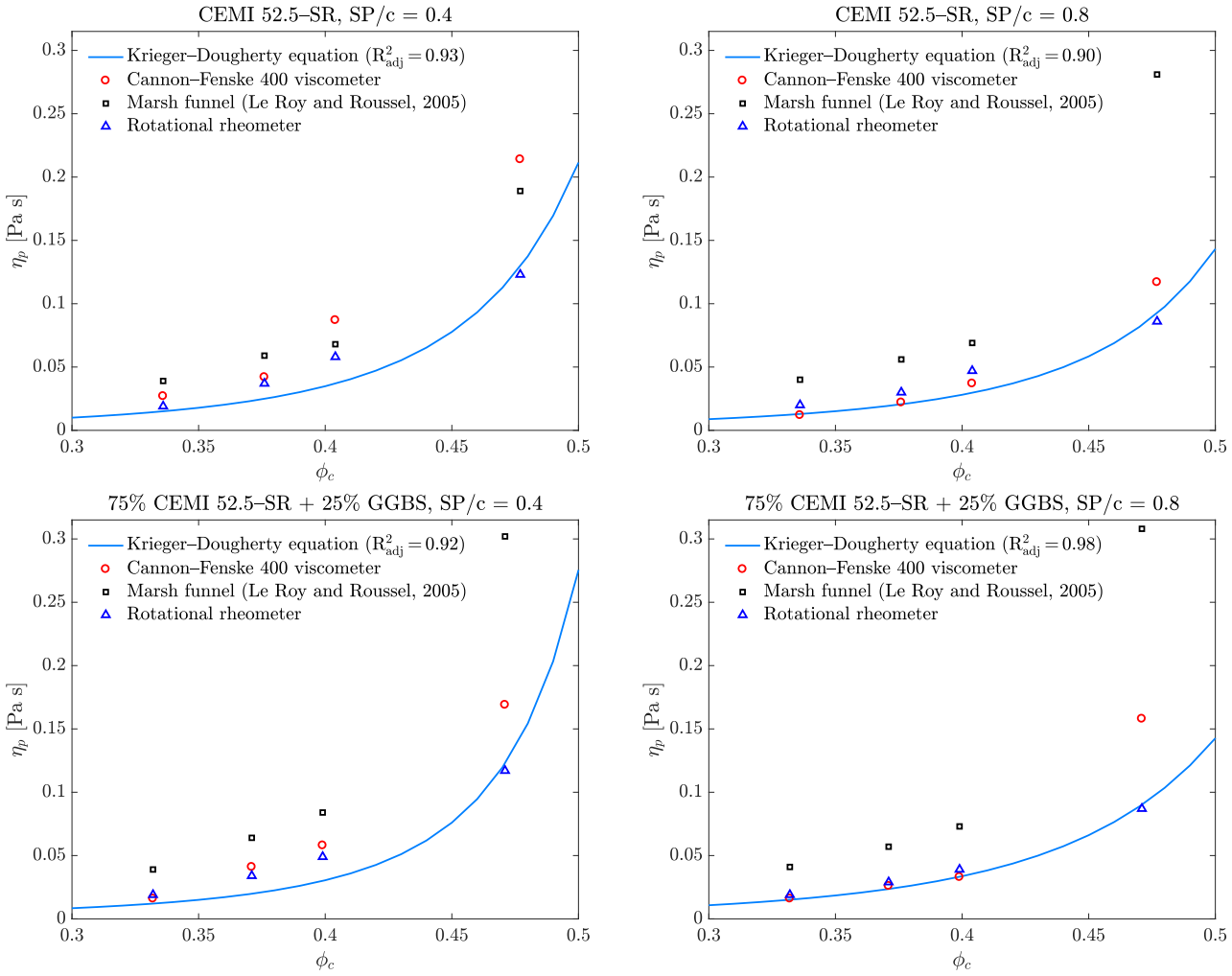

Figure 7: Calculated values of η_p and comparison between measuring instruments (CEM I 52.5–SR and 75% CEM I 52.5–SR + 25% GGBS). Fit to the Krieger and Dougherty equation obtained with rotational rheometer data (continuous line).

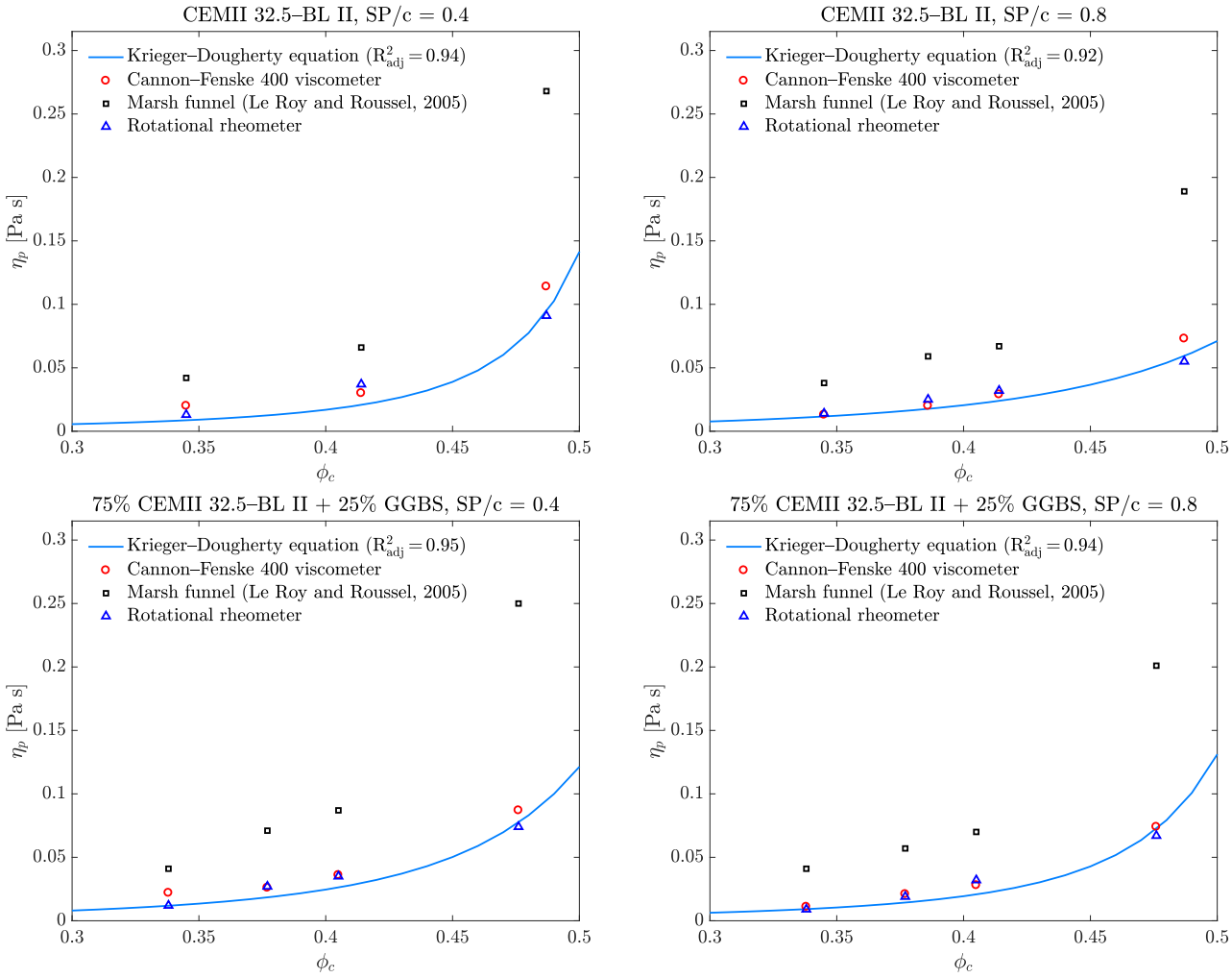

Figure 8: Calculated values of η_p and comparison between measuring instruments (CEM II 32.5–BL II and 75% CEM II 32.5–BL II + 25% GGBS). Fit to the Krieger and Dougherty equation obtained with rotational rheometer data (continuous line).

Cementitious material	*SP*/*c*	$\eta_{\mathrm{w}}[\mathrm{mPa\,s}]$	ϕ_{m}	95% CI	$[\eta]$	95% CI	R^2_{adj}
CEM I 52.5–SR	0.4	0.933	0.68	0.43–0.93	6.6	4.4–7.7	0.93
	0.8	0.933	0.70	0.41–0.98	6.4	3.9–7.4	0.90
	1.0	0.891	0.75	0.56–0.94	6.8	5.5–7.7	0.98
	1.2	0.891	0.69	0.62–0.76	6.5	5.9–6.9	0.99
CEM II 32.5 BL–II	0.4	0.933	0.57	0.53–0.61	5.0	4.6–5.3	0.94
	0.8	0.933	0.83	0.54–1.00	6.2	4.8–6.8	0.92
75% CEM I 52.5–SR + 25% GGBS	0.4	0.933	0.60	0.36–0.84	6.0	2.8–7.3	0.98
	0.8	0.933	0.83	0.50–1.00	6.5	4.8–7.3	0.99
75% CEM II 32.5 BL–II + 25% GGBS	0.4	0.933	0.69	0.26–1.00	6.0	0.2–7.3	0.95
	0.8	0.933	0.51	0.45–0.56	4.3	3.6–4.9	0.94

Table 2: Adjustment of the parameters of the Krieger and Dougherty equation (Eq. 23), ϕ_m and $[\eta]$, from measurements with the rotational rheometer (measuring range: $0-600\ \mathrm{s}^{-1}$; CI stands for confidence interval).

SP/c = 0.4 and 1.2 (admixture based on polycarboxylates and poly–aryl–ether, respectively) and higher for *SP*/c = 0.8 and 1.0 (admixture based on polycarboxylates and poly–aryl–ether, respectively).

Regarding the results obtained in cement pastes with polycarboxylate–based superplasticizer admixture (Table 4), it can be seen that the model proposed by Le Roy and Roussel gives the highest values of η_p in relation to the other models and the rotational rheometer. This overestimation is very notable with respect to the rotational rheometer's measurements (it approximately doubles the values) and is increased even more in high concentrations of cementitious particles, ϕ_c. The models of Guria *et al.* and Balhoff *et al.* offer the best approximations in relation to the rotational rheometer, mainly with low admixture content (*SP*/c = 0.4), increasing the difference between η_p values as ϕ_c increases when an *SP*/c = 0.8 ratio is used. The model of Guria *et al.* always predicts higher η_p values than that of Balhoff *et al.* The Sedaghat and Pitt models only show results from a certain concentration of solids (ϕ_c = 0.404 and 0.477). For both amounts of superplasticizer, it can be seen how the results of the Pitt model [52] approximate those of the rotational rheometer. In contrast, the Sedaghat model [53] grossly underestimates its η_p predictions.

Concerning pastes with poly–aryl–ether superplasticizer admixture (Table 4), the model of Le Roy and Roussel again overestimate their results with respect to rotational rheometer measurements for the two admixture contents (*SP*/c = 1.0 and 1.2). Also, the models of Guria *et al.* and Balhoff *et al.* are closer to the measurements of the rotational rheometer in both amounts of superplasticizer. However, they show relevant overestimations for high concentrations of cementitious particles (ϕ_c = 0.477) and admixture dose *SP* /c = 0.4. The Sedaghat and Pitt models again offer η_p results only from ϕ_c = 0.404 and 0.477. In this case, the two models significantly underestimate the η_p values with respect to those obtained with the rotational rheometer, in particular the Sedaghat model.

According to what was found in the application of the models, several considerations can be made. The Sedaghat and Pitt models provide the worst approximations for rotational rheometer measurements. The parameter t_f requires exceeding a minimum to obtain a value of η_p ($t_f \geq 26$ s for the Sedaghat model, through the dimensionless flow coefficient K, which must be less than the unit to represent the consistency curve, and $t_f \geq 24.5$ s in the Pitt model). It should be noted here that both the Sedaghat and Pitt models are adjusted for suspension volumes equal to 1.5 dm^3 and 0.946 dm^3, respectively. In addition, another explanation for the low values of η_p calculated with the Sedaghat model maybe that, as the author suggests, the coefficients b_i, c_i for the calculation of K can be improved and calibrated using new $H - t_f$ curves for the actual cementitious suspensions used, for the volume of filling and drainage (0.8 dm^3 and 0.4 dm^3, respectively) and for the

Cementitious material	w/c	*SP*/c	ϕ_c	η_p [Pa s]		
				RR	C–F 400	MF$^{(*)}$
CEM I 52.5–SR	0.35	0.4	0.477	0.123	0.214	0.189
	0.35	0.8	0.477	0.086	0.117	0.281
	0.47	0.4	0.404	0.058	0.087	0.068
	0.47	0.8	0.404	0.047	0.037	0.069
	0.53	0.4	0.376	0.037	0.042	0.059
	0.53	0.8	0.376	0.030	0.022	0.056
	0.63	0.4	0.336	0.019	0.027	0.039
	0.63	0.8	0.336	0.020	0.012	0.040
CEM II 32.5 BL–II	0.35	0.4	0.487	0.091	0.114	0.268
	0.35	0.8	0.487	0.055	0.073	0.189
	0.47	0.4	0.414	0.037	0.030	0.066
	0.47	0.8	0.414	0.032	0.029	0.067
	0.53	0.8	0.386	0.025	0.020	0.059
	0.63	0.4	0.345	0.013	0.020	0.042
	0.63	0.8	0.345	0.014	0.013	0.038
75% CEM I 52.5–SR + 25% GGBS	0.35	0.4	0.471	0.117	0.169	0.302
	0.35	0.8	0.471	0.087	0.158	0.308
	0.47	0.4	0.399	0.049	0.058	0.084
	0.47	0.8	0.399	0.039	0.033	0.073
	0.53	0.4	0.371	0.034	0.041	0.064
	0.53	0.8	0.371	0.029	0.026	0.057
	0.63	0.4	0.332	0.019	0.016	0.039
	0.63	0.8	0.332	0.019	0.016	0.041
75% CEM II 32.5 BL–II + 25% GGBS	0.35	0.4	0.476	0.074	0.087	0.250
	0.35	0.8	0.476	0.067	0.074	0.201
	0.47	0.4	0.405	0.035	0.036	0.087
	0.47	0.8	0.405	0.032	0.028	0.070
	0.53	0.4	0.377	0.027	0.026	0.071
	0.53	0.8	0.377	0.019	0.021	0.057
	0.63	0.4	0.338	0.012	0.022	0.041
	0.63	0.8	0.338	0.009	0.011	0.041

$^{(*)}$Using the model of Le Roy & Roussel [16, 32]

Table 3: Plastic viscosity values in cement pastes measured with different instruments (RR, C–F and MF stand for rotational rheometer, Cannon–Fenske viscometer and Marsh funnel, respectively).

w/c	*SP*/c	ϕ_c	RR, η_p [Pa s]	Marsh funnel, η_p [Pa s]				
				Le Roy–Roussel	Guria *et al.*	Balhoff *et al.*	Sedaghat	Pitt
0.35	0.4	0.477	0.123	0.376	0.256	0.141	0.043	0.140
0.35	0.8	0.477	0.086	0.289	0.195	0.195	0.032	0.119
0.40	1.0	0.443	0.091	0.140	0.230	0.231	0.020	0.067
0.40	1.2	0.443	0.086	0.105	0.119	0.119	0.006	0.022
0.47	0.4	0.404	0.058	0.093	0.048	0.044	0.005	0.019
0.47	0.8	0.404	0.047	0.088	0.118	0.110	0.005	0.019
0.47	1.0	0.404	0.054	0.093	0.080	0.074	0.006	0.021
0.47	1.2	0.404	0.048	0.076	0.034	0.036	0.003	0.014
0.53	0.4	0.376	0.037	0.060	0.027	0.025	–	–
0.53	0.8	0.376	0.030	0.057	0.049	0.045	–	–
0.53	1.0	0.376	0.034	0.062	0.035	0.032	–	–
0.53	1.2	0.376	0.032	0.053	0.030	0.028	–	–
0.63	0.4	0.336	0.019	0.040	0.023	0.021	–	–
0.63	0.8	0.336	0.020	0.043	0.023	0.023	–	–
0.63	1.0	0.336	0.014	0.042	0.017	0.016	–	–
0.63	1.2	0.336	0.015	0.042	0.004	0.003	–	–

Table 4: Plastic viscosity values of cement pastes (made with CEM I 52.5–SR only) calculated with different models applied to the Marsh funnel. The cement suspensions with 0.4 and 0.8 *SP*/c ratios correspond to the polycarboxylate type superplasticizer admixture modified in aqueous base, whereas *SP*/c ratios of 1.0 and 1.2 correspond to the superplasticizer of the poly–aryl–ether type.

dimensions of the Marsh funnel [53]. This model offers good approximations in Newtonian fluids, although a deepening of experimental validation is necessary, especially for non–Newtonian suspensions (of Bingham type rheological behavior, as is the case with cement pastes) [53].

Le Roy and Roussel [16] also say that if t_f is less than 12 s there is no linear relationship between η_p and t_f. In these cases where the values of t_f and, consequently, η_p are low, it is necessary to choose a smaller diameter of the Marsh funnel capillary.

For these reasons, it is essential to understand the measuring range of the Marsh funnel according to its geometric characteristics and depending on the rheological behavior of the material to be studied (diameter of the capillary of the instrument, measurement intervals of rheological parameters of the suspension and solid particle size distribution). It is also essential to understand the principles that underlie the derived equations for the model to be applied.

5 Conclusions

Knowledge of the rheological behavior of cementitious materials is important in digital fabrication technologies and casting processes. Besides, plastic viscosity is a principal parameter for self–compacting concrete mix design methods based on rheological criteria. This research deals with the measurement of plastic viscosity in cement pastes using capillary–type viscometers, which are simpler and cheaper devices than rotational rheometers. Plastic viscosity measurements were also made using a rotational rheometer that served as a reference to compare the values obtained with each instrument.

To this end, a total of 39 cement pastes of different compositions were designed in terms of cement, mineral addition and superplasticizer admixture, with various water–cementitious materials ratios, which can

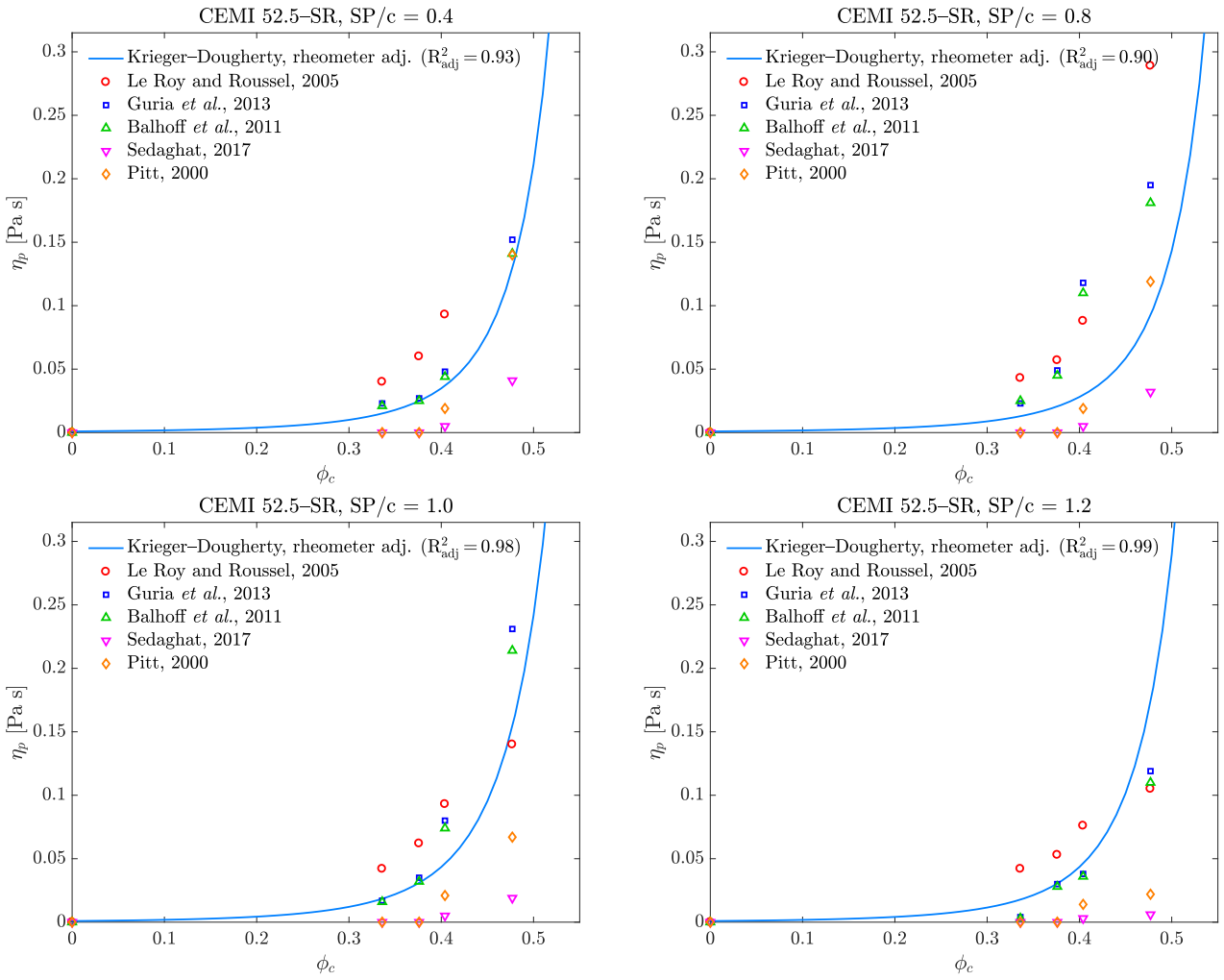

Figure 9: Calculated values of η_p obtained with the Marsh funnel and comparison between models. Adjustment curve of the Krieger and Dougherty equation to the measurements of the rotational rheometer (pastes with admixture based on polycarboxylates and poly–aryl–ether).

serve as starting data for use in high–performance concrete design methods based on rheological models. The results show that the Cannon–Fenske viscometer offers a better approximation of the plastic viscosity value of cement pastes (CEM I 52.5–SR, CEM II 32.5 BL–II, 75% CEM I 52.5–SR and 25% GGBS, 75% CEM II 32.5 BL–II and 25% GGBS, with superplasticizer admixture based on modified polycarboxylates in water base) than the Marsh funnel when applying the Le Roy and Roussel model, with respect to the rheological measurement made with the rotational rheometer. Regarding the comparison between models, the models of Guria *et al.* and Balhoff *et al.* provide the best approximations of the plastic viscosity of the cement pastes (CEM I 52.5–SR, with superplasticizer admixture of poly–aryl–ether type) concerning the measurements with the rotational rheometer. The Sedaghat and Pitt models calculate plastic viscosity values well below those measured with the rotational rheometer, offering only results from high concentrations of solid cementitious particles (corresponding to low water–cementitious materials ratios). However, it should be considered that the parameters of these models are adjusted to certain volumes and sample characteristics that are not optimum for the pastes used here.

These results are consistent with the fundamentals that govern the operation of capillary viscometers in which the selection of the capillary diameter is the most important parameter to take into account according to the characteristics of the material to be tested (rheological behavior and size distribution of particles). In addition, in line with the results obtained, the application of the models for the Marsh funnel suggests a good understanding of the principles and hypotheses from which their equations derive, as well as the need to adjust some of the parameters used according to the type of suspension you are experimenting with.

From this study, the usefulness of capillary viscometers in the measurement of viscosity in cement pastes for self–compacting concrete as alternative instruments to rotational rheometers is highlighted, proposing a series of recommendations according to the apparatus and model used. However, whatever the device used, it is essential to express the results obtained for plastic viscosity by referring to the characteristics of the measuring instrument and the test performed, as well as the preparation conditions and mixing protocols, since this rheological parameter is dependent on a multitude of factors.

Finally, it would be appropriate to extend the experimentation in this type of suspensions using new paste compositions to broaden the validity range of the conclusions drawn in this investigation and to adjust the parameters of some of the models shown, in particular those giving worse approaches with respect to measurements made with the rotational rheometer.

6 Acknowledgements

The authors appreciate the funding received from the *Ministerio de Innovación, Ciencia y Universidades*, Spain, through BIA2015–68678–C2–1–R, BIA2016–75431–R and RTC–2017–6736–3 projects. We especially want to thank *Cementos Portland Valderrivas*, *Cementos Tudela Veguín*, SIKA, and BASF for the complimentary supply of materials. Ángel de la Rosa also acknowledges the FPI BES–2016–077458 scholarship from the *Ministerio de Innovación, Ciencia y Universidades*, Spain.

References

[1] D. Feys, R. Verhoeven, and G. De Schutter. Why is fresh self–compacting concrete shear thickening? *Cement and Concrete Research*, 39:510–523, 2009.

[2] J.E. Wallevik. The particle flow interaction. theory–thixotropic behavior and structural breakdown. In *36 Conference on Our World in Concrete Structures, Singapore*, pages 1–7, 2011.

[3] N. Roussel, G. Ovarlez, S. Garrault, and C. Brumaud. The origins of thixotropy of fresh cement pastes. *Cement and Concrete Research*, 42:148–157, 2012.

[4] R. Shaughnessy. The rheological behavior of fresh cement pastes. *Cement and Concrete Research*, 18:327–341, 1988.

[5] A.W. Saak, H.M. Jennings, and S.P. Shah. Characterization of the rheological properties of cement paste for use in self–compacting concrete. In *1st International RILEM Symposium on Self-Compacting Concrete, Stockholm*. RILEM, 1999.

[6] O.H. Wallevik and M.R. Geiker. Course on the rheology of cement based particle suspensions. In *Lecture notes, Copenhagen*, 2007.

[7] M. Cyr, Legrand C., and M. Mouret. Study of the shear thickening effect of superplasticizers on the rheological behaviour of cement pastes containing or not mineral additives. *Cement and Concrete Research*, 30:1477–1483, 2000.

[8] R.L. Hoffman. Explanations for the cause of shear thickening in concentrated colloidal suspensions. *Journal of Rheology*, 42(1):111–123, 1998.

[9] R.L. Hoffman. Discontinuous and dilatant viscosity behavior in concentrated suspensions: I. Observations of a flow instability. *Transactions of the Society of Rheology*, 16:155–173, 1972.

[10] R.L. Hoffman. Discontinuous and dilatant viscosity behavior in concentrated suspensions: II. Theory and experimental tests. *Journal of Colloid Interface Science*, 46(3):491–506, 1974.

[11] V.H. Nguyen, S. Remond, and J.L. Gallia. Influence of cement grouts composition on the rheological behaviour. *Cement and Concrete Research*, 41:292–300, 2011.

[12] A. Yahia. Effect of solid concentration and shear rate on shear–thickening response of high–performance cement. *Construction and Building Materials*, 53:517–521, 2014.

[13] A. Yahia. Shear–thickening behavior of high–performance cement grouts. Influencing mix–design parameters. *Cement and Concrete Research*, 41:230–235, 2011.

[14] J.E. Wallevik. Rheological properties of cement paste: thixotropic behavior and structural breakdown. *Cement and Concrete Research*, 39:14–29, 2009.

[15] N. Roussel. Steady and transient flow behaviour of fresh cement pastes. *Cement and Concrete Research*, 35:1656–1664, 2005.

[16] N. Roussel and R. Le Roy. The Marsh cone: a test or a rheological apparatus? *Cement and Concrete Research*, 35:823–830, 2005.

[17] M.A. Rahman and M. Nehdi. Effect of geometry, gap and surface friction of test accesory on measured rheological properties of cement paste. *ACI Materials Journal*, 100(4), 2003.

[18] F. Toussaint, C. Roy, and P.H. Jézéquel. Reducing shear thickening of cement–based suspensions. In *Workshop on Rheophysics, Paris*, 2008.

[19] D.A. Williams, A.W. Saak, and H.M. Jennings. The influence of mixing on the rheology of fresh cement paste. *Cement and Concrete Research*, 29:1491–1496, 1999.

[20] F. Puertas, H. Santos, M. Palacios, and S. Martínez-Ramírez. Polycarboxylate superplasticiser admixtures: effect on hydratation, microstructure and rheological behaviour in cement pastes. *Advances in Cement Research*, 17(2):77–89, 2005.

[21] C. Jayasree and R. Gettu. Experimental study of the flow behaviour of superplasticized cement paste. *Materials and Structures*, 41:1581–1593, 2008.

[22] M.M. Cross. Rheology of non-Newtonian fluids: a new flow equation for pseudoplastic systems. *Journal of Colloid Science*, 20:417–437, 1965.

[23] G.H. Tattersall. Structural breakdown of cement pastes at constant rate of shear. *Nature*, 175(166), 1955.

[24] P.F.G. Banfill and D.C. Saunders. On the viscometric examination of cement pastes. *Cement and Concrete Research*, 11:363–370, 1981.

[25] A. Papo. Rheological models for cement pastes. *Materials and Structures*, 21:41–46, 1988.

[26] N. Roussel, A. Lemaître, P. Flatt, and P. Coussot. Steady state flow of cement suspensions: a micromechanical state of the art. *Cement and Concrete Research*, 40:77–84, 2010.

[27] O. Burgos-Montes, M.M. Alonso, and F. Puertas. Viscosity and water demand of limestone –and fly ash– blended cement pastes in the presence of superplasticisers. *Construction and Building Materials*, 48:417–423, 2013.

[28] T. Muhua and D.M. Roy. An investigation of the effect of organic solvent on the rheological properties and hydration of cement paste. *Cement and Concrete Research*, 17(6):983–994, 1987.

[29] C. Atzeni, L. Massidda, and U. Sanna. Comparison between rheological models for portland cement pastes. *Cement and Concrete Research*, 15:511–519, 1985.

[30] H.A. Barnes. Shear–thickening (dilatancy) in suspensions of non–aggregating solid particles dispersed in Newtonian liquids. *Journal of Rheology*, 33:329, 1989.

[31] M.M. Alonso, M. Palacios, and F. Puertas. Compatibility between polycarboxylate–based admixtures and blended–cement pastes. *Cement and Concrete Composites*, 35:151–162, 2013.

[32] R. Le Roy and N. Roussel. The Marsh cone as viscometer: theoretical analysis and practical limits. *Materials and Structures*, 38:25–30, 2005.

[33] L. Struble and G.K. Sun. Viscosity of portland cement pastes as a function of concentration. *Advanced Cement Based Materials*, 2:62–69, 1995.

[34] D. Feys, R. Cepuritis, S. Jacobsen, K. Lesage, E. Secrieru, and A. Yahia. Measuring rheological properties of cement pastes: most common techniques, procedures and challenges. *RILEM Technical Letters*, 2:129–135, 2017.

[35] R. Moreno Botella. *Reología de suspensiones cerámicas*. Consejo Superior de Investigaciones Científicas, Madrid, 2005.

[36] N. Roussel. A thixotropy model for fresh fluid concretes: theory, validation and applications. *Cement and Concrete Research*, 36:1797–1806, 2006.

[37] L. Ferrara, M. Cremonesi, N. Tregger, A. Frangi, and S.P. Shah. On the identification of rheological properties of cement suspensions: Rheometry, computational fluid dynamics modeling and field test measurements. *Cement and Concrete Research*, 42:1134–1146, 2012.

[38] C. Menna, J. Mata-Falcón, F.P. Bosc, G. Vantyghemd, L. Ferrara, D. Aspronea, T. Saletc, and W. Kaufmann. Opportunities and challenges for structural engineering of digitally fabricated concrete. *Cement and Concrete Research*, 133:106079, 2020.

[39] N. Roussel. Rheological requirements for printable concretes. *Cement and Concrete Research*, 112:76–85, 2018.

[40] H. Jeong, S.J. Han, S.H. Choi, Y.L. Lee, S.T. Yi, and K.S. Kim. Rheological property criteria for buildable 3d printing concrete. *Materials*, 12:657, 2019.

[41] E. Secrieru, W. Mohamed, S. Fataei, and V. Mechtcherine. Assessment and prediction of concrete ow and pumping pressure in pipeline. *Cement and Concrete Composites*, 107:103495, 2020.

[42] S. Fataei, E. Secrieru, and V. Mechtcherine. Experimental insights into concrete flow–regimes subject to shear–induced particle migration (sipm) during pumping. *Materials*, 13:1233, 2020.

[43] M. S. Abo Dhaheer, M. M. Al-Rubaye, W. S. Alyhya, B. L. Karihaloo, and S. Kulasegaram. Proportioning of self–compacting concrete mixes based on target plastic viscosity and compressive strength: Part I – Mix design procedure. *Journal of Sustainable Cement–Based Materials*, 5(4):199–216, 2016.

[44] Á. de la Rosa, E. Poveda, G. Ruiz, and H. Cifuentes. Proportioning of self-compacting steel-fiber reinforced concrete mixes based on target plastic viscosity and compressive strength: Mix-design procedure and experimental validation. *Construction and Building Materials*, 189:409–419, 2018.

[45] M.R. Cannon and M.R. Fenske. Viscosity measurement. *Industrial and Engineering Chemistry Analytical Edition*, 10(6):297–301, 1938.

[46] M.R. Cannon, R.E. Manning, and J.R. Bell. Viscosity measurement. Kinetic energy connection and new viscometer. *Analytical Chemistry*, 32(3):355–358, 1960.

[47] H. Noureddini, B.C. Teoh, and L.D. Clements. Viscosities of vegetable oils and fatty acids. *Journal of the American Oil Chemistry Society*, 69(12):1189–1191, 1992.

[48] J.B. Segur and H.E. Oberstar. Viscosity of glycerol and its aqueous solutions. *Industrial and Engineering Chemistry*, 43(9):2117–2120, 1951.

[49] J. Liu, M.D. Nguyen, J.D. Andy, and S.J. Shire. Reversible self-association increases the viscosity of a concentrated monoclonal antibody in aqueous solution. *Journal of Pharmaceutical Sciences*, 94(9):1928–1940, 2005.

[50] D.P. Bentz. Influence of shrinkage-reducing admixtures on early–age properties of cement pastes. *Journal of Advanced Concrete Technology*, 4(3):423–429, 2006.

[51] H.N. Marsh. Properties and treatment of mud. Petroleum development technology. *Transaction of AIME*, pages 234–315, 1931.

[52] M.J. Pitt. The Marsh funnel and drilling fluid viscosity: a new equation for field use. *SPE Drilling and Completion*, 15(1):3–6, 2000.

[53] A. Sedaghat. A novel and robust model for determining rheological properties of Newtonian and non-Newtonian fluids in a Marsh funnel. *Journal of Petroleum Science and Engineering*, 156:896–916, 2017.

[54] F.H.M. Almahdawi, A.Z. Al-Yaseri, and N. Jasi. Apparent viscosity direct from Marsh funnel test. *Iraqi Journal of Chemical and Petroleum Engineering*, 15(1):51–57, 2014.

[55] C. Guria, R. Kumar, and P. Mishra. Rheological analysis of drilling fluid using Marsh funnel. *Journal of Petroleum Science and Engineering*, 105:62–69, 2013.

[56] B. Schoesser and M. Thewes. Marsh funnel testing for rheology analysis of bentonite slurries for slurry shields. In *ITA WTC 2015 Congress and 41st General Assembly*. ITA WTC, 2015.

[57] B. Schoesser and M. Thewes. Do we tap the full potential from Marsh funnel tests? Rheology testing for bentonite suspensions. *Tunneling Journal*, 2015.

[58] K. Liu, Z. Qiu, Y. Luo, and G. Zhou. Measure rheology of drilling fluids with Marsh funnel viscometer. *Drilling Fluid and Completion Fluid*, 31(5):60–62, 2014.

[59] H.A. Abdulrahman. Calculation rheological properties of water base mud using Marsh funnel. In *B.Sc. Dissertation*. Sudan University of Science and Technology, Sudan, 2015.

[60] A. Sedaghat, M.A.A. Omar, S. Damrah, and M. Gaith. Mathematical modelling of the flow rate in a Marsh funnel. *Journal of Energy Technology Research*, 1(1):1–12, 2016.

[61] Z. Li, L. Zheng, and W. Huang. Rheological analysis of newtonian and non-newtonian fluids using marsh funnel: Experimental study and computational fluid dynamics modeling. *Energy Science and Engineering*, 00:1–19, 2020.

[62] L. D'Aloia Schwartzentruber, R. Le Roy, and J. Cordin. Rheological behaviour of fresh cement pastes formulated from a self compacting concrete (SCC). *Cement and Concrete Research*, 36:1203–1213, 2006.

[63] V.H. Nguyen, S. Rémond, J.L. Gallias, J.P. Bigas, and P. Muller. Flow of Herschel-Bulkley fluids through the Marsh cone. *Journal of Non-Newtonian Fluid Mechanics*, 139(1–2):128–134, 2006.

[64] B. Schoesser and M. Thewes. See tunnel: Promoting tunneling in see region. In *ITA WTC 2015 Congress and 41st General Assembly, Dubrovnik*. ITA WTC, 2015.

[65] M. Cremonesi, L. Ferrara, A. Frangi, and U. Parego. Simulation of the flow of fresh cement suspensions by a lagrangian finite element approach. *Journal of Non–Newtonian Fluid Mechanics*, 165:1555–1563, 2010.

[66] M.T. Balhoff, L.W. Lake, P.M. Bommer, R.E. Lewis, M.J. Weber, and J.M. Calderin. Rheological and yield stress measurements of non-Newtonian fluids using a Marsh funnel. *Journal of Petroleum Science and Engineering*, 77:393–402, 2011.

[67] M.H. Mohammed, R. Pusch, S. Knutsson, and Hellström. Influence of particle size distributions on yield stress and viscosity of cement–fly ash pastes. *Engineering*, 6:217–229, 2014.

[68] I.M. Krieger and T.J. Dougherthy. A mechanism for non–Newtonian flow in suspensions of rigid spheres. *Journal of Rheology*, 3:137–152, 1959.

[69] J.A. Brydson. *Flow properties of polymer melts*. George Goodwin, London, 1981.

[70] API American Petroleum Institute, West Conshohocken, PA. *API 13B–1: 2009–03: Recommended Practice for field testing of waterbased drilling fluids*, 4th edition edition, 2009.

[71] DIN Deutsches Institut für Normung e.V., Berlin. *DIN 4127:2014–02: Earthworks and foundation engineering. Test methods for supporting fluids used in the construction of diaphragm walls and their constituent products*, 2014.

[72] F. Puertas, M.M. Alonso, and T. Vázquez. Effect of polycarboxylate admixtures on Portland cement paste setting and rheological behaviour. *Materiales de Construcción*, 55(277):61–73, 2005.

[73] M.M. Alonso, M. Palacios, F. Puertas, A.G. De la Torre, and M.A.G. Aranda. Effect of polycarboxylate admixture structure on cement paste rheology. *Materiales de Construcción*, 57(286):65–81, 2007.

[74] ASTM International. *ASTM C305–99, Standard Method of Test for Mechanical Mixing of Hydraulic Cement Pastes and Mortars of Plastic Consistency*, 2004.

[75] ASTM International. *AASHTO T162–04, Standard Method of Test for Mechanical Mixing of Hydraulic Cement Pastes and Mortars of Plastic Consistency*, 2004.

[76] D. Jiao, C. Shi, and Q. Yuan. Time–dependent rheological behavior of cementitious paste under continuous shear mixing. *Construction and Building Materials*, 226:591–600, 2019.

[77] P.V.P. Moorthi, F. Pra Mio, P. Nanthagopalan, and L. Ferrara. Onset and intensity of shear thickening in cementitious suspensions–A parametrical study. *Construction and Building Materials*, 244:118292, 2020.

[78] ASTM International, West Conshohocken, PA. *ASTM D445-17a, Standard Test Method for Kinematic Viscosity of Transparent and Opaque Liquids (and Calculation of Dynamic Viscosity)*, 2017.

[79] British Standards Institute. *BS EN 445:2007. Grout for prestressing tendons. Test methods*, 2007.

[80] ASTM International, West Conshohocken, PA. *ASTM C939 / C939M-16a, Standard Test Method for Flow of Grout for Preplaced–Aggregate Concrete (Flow Cone Method)*, 2016.

[81] AENOR, Madrid. *Ejecución de trabajos geotécnicos especiales. Inyecciones*, 2001.

[82] AENOR. *UNE–EN 1015–6, Métodos de Ensayo de los Morteros para Albañilería. Parte 6, Determinación de la Densidad Aparente del Mortero Fresco*, 1999.

[83] MATLAB. `www.mathworks.com`, 2016.

Data Annex

Experimental measurements made with the double cone–plate rotational rheometer

Individual measurements of plastic viscosity, η_p, obtained with the rotational rheometer can be seen in Table 5.

Cementitious material	*SP* type	w/c	*SP*/c	ϕ_c	ρ_p [$\mathrm{kg/m^3}$]	η_p [Pa s]	R^2
CEM I 52.5–SR	Polycarboxylate	0.35	0.4	0.477	2001	0.123	0.997
		0.35	0.8	0.477	2025	0.086	0.997
		0.47	0.4	0.404	1864	0.058	0.996
		0.47	0.8	0.404	1828	0.047	0.998
		0.53	0.4	0.376	1776	0.037	0.995
		0.53	0.8	0.376	1772	0.030	0.994
		0.63	0.4	0.336	1602	0.019	0.954
		0.63	0.8	0.336	1743	0.020	0.964
CEM I 52.5–SR	Poly–aryl–ether	0.40	1.0	0.443	1934	0.091	0.998
		0.40	1.2	0.443	1962	0.086	0.997
		0.47	1.0	0.404	1856	0.054	0.998
		0.47	1.2	0.404	1842	0.048	0.999
		0.53	1.0	0.376	1816	0.034	0.994
		0.53	1.2	0.376	1821	0.032	0.991
		0.63	1.0	0.336	1728	0.014	0.886
		0.63	1.2	0.336	1728	0.015	0.900
CEM II 32.5 BL–II	Polycarboxylate	0.35	0.4	0.487	1989	0.091	0.994
		0.35	0.8	0.487	2001	0.055	0.999
		0.47	0.4	0.414	1814	0.037	0.992
		0.47	0.8	0.414	1864	0.032	0.991
		0.53	0.8	0.376	1776	0.025	0.970
		0.63	0.4	0.345	1713	0.013	0.827
		0.63	0.8	0.345	1602	0.014	0.850
75% CEM I 52.5–SR + 25% GGBS	Polycarboxylate	0.35	0.4	0.471	1993	0.117	0.999
		0.35	0.8	0.471	1997	0.087	0.993
		0.47	0.4	0.399	1854	0.049	0.996
		0.47	0.8	0.399	1844	0.039	0.999
		0.53	0.4	0.371	1778	0.034	0.994
		0.53	0.8	0.371	1784	0.029	0.992
		0.63	0.4	0.438	1642	0.019	0.954
		0.63	0.8	0.438	1706	0.019	0.964
75% CEM II 32.5 BL–II + 25% GGBS	Polycarboxylate	0.35	0.4	0.476	1967	0.074	0.998
		0.35	0.8	0.476	1989	0.067	0.998
		0.47	0.4	0.405	1820	0.035	0.994
		0.47	0.8	0.405	1818	0.032	0.991
		0.53	0.4	0.377	1771	0.027	0.976
		0.53	0.8	0.377	1741	0.019	0.931
		0.63	0.4	0.338	1725	0.012	0.826
		0.63	0.8	0.338	1695	0.009	0.697

Table 5: Physical and rheological properties of pastes. Measuring range in rotational rheometer: $0-600\ \mathrm{s^{-1}}$

Experimental measurements performed with the Marsh funnel

Tables 6-9 array all the individual measurements performed with the Marsh funnel, plus the corresponding plastic viscosity obtained with the model of Le Roy and Roussel (Eqs. 6 and 7) [16, 32]. Each paste was measured two consecutive times. In all cases, $0.8\,\mathrm{dm}^3$ of suspension are introduced, and $0.4\,\mathrm{dm}^3$ are drained.

w/c	*SP*/*c*	ϕ_c	ρ_p [kg/m^3]	T [°C]	H_0 [m]	H [m]	t_f [s]	η_p [Pa s]	$t_{f,\mathrm{av}}$ [s]	$\eta_{p,\mathrm{av}}$ [Pa s]
0.35	0.4	0.477	2001	20.6	0.226	0.177	73	0.189	73	0.189
0.35	0.4	0.477	2001	20.6	0.226	0.177	72	0.188		
0.35	0.8	0.477	2025	21.0	0.226	0.177	117	0.309	107	0.281
0.35	0.8	0.477	2025	21.0	0.226	0.175	96	0.253		
0.47	0.4	0.404	1864	20.3	0.223	0.172	27	0.066	29	0.068
0.47	0.4	0.404	1864	20.3	0.225	0.175	28	0.069		
0.47	0.8	0.404	1828	20.9	0.226	0.177	29	0.068	30	0.069
0.47	0.8	0.404	1828	20.9	0.225	0.175	30	0.070		
0.53	0.4	0.376	1776	20.2	0.224	0.174	28	0.063	26	0.059
0.53	0.4	0.376	1776	20.2	0.225	0.175	24	0.054		
0.53	0.8	0.376	1772	20.9	0.225	0.175	25	0.057	25	0.056
0.53	0.8	0.376	1772	20.9	0.224	0.174	24	0.054		
0.63	0.4	0.336	1602	20.5	0.221	0.169	19	0.039	19	0.039
0.63	0.4	0.336	1602	20.5	0.220	0.167	19	0.038		
0.63	0.8	0.336	1743	20.9	0.225	0.175	18	0.040	18	0.040
0.63	0.8	0.336	1743	20.9	0.225	0.175	17	0.040		

Table 6: Parameters measured with the Marsh funnel for paste made with CEM I 52.5–SR. Volume introduced, $0.8\,\mathrm{dm}^3$; drained volume, $0.4\,\mathrm{dm}^3$.

Experimental measurements made with the Cannon–Fenske 400 viscometer

Tables 10-13 array all the individual measurements performed with the Cannon–Fenske viscometer (400 series). In congruence with Marsh funnel measurements, each of the pastes was tested twice on the Cannon–Fenske viscometer. These tables include the density, times of passage through the viscometer bulbs, the constants of each viscometer bulb according to the test temperature at which it was performed and the plastic viscosity (which is already an average value of the two bulbs according to Eqs. 20 and 21).

Experimental measurements for comparing the plastic viscosity of CEM I 52.5–SR cement paste made with Marsh funnel according to different authors

To compare the calculated results with the various equations in the scientific literature that use the Marsh funnel (Le Roy and Roussel —the only ones using cement pastes—, Sedaghat, Guria *et al.*, Balhoff *et al.* and Pitt —corresponding to investigations carried out with non–Newtonian suspensions different from cement pastes—), new CEM I 52.5–SR pastes were manufactured and then measured with the Marsh funnel, the test measurement data being the expressed in Table 14. The plastic viscosity figures corresponding to these experimental data are in Table 4.

w/c	*SP*/c	ϕ_c	ρ_p [kg/m^3]	T [°C]	H_0 [m]	H [m]	t_f [s]	η_p [Pa s]	$t_{f,\mathrm{av}}$ [s]	$\eta_{p,\mathrm{av}}$ [Pa s]
0.35	0.4	0.471	1993	19.7	0.226	0.177	110	0.288	117	0.302
0.35	0.4	0.471	1993	19.7	0.226	0.177	122	0.317		
0.35	0.8	0.471	1997	19.6	0.226	0.177	117	0.306	119	0.308
0.35	0.8	0.471	1997	19.6	0.225	0.175	120	0.311		
0.47	0.4	0.399	1854	19.7	0.225	0.175	35	0.083	36	0.084
0.47	0.4	0.399	1854	19.7	0.225	0.175	36	0.086		
0.47	0.8	0.399	1844	20.6	0.225	0.175	30	0.073	30	0.073
0.47	0.8	0.399	1844	20.6	0.226	0.177	30	0.073		
0.53	0.4	0.371	1778	19.7	0.225	0.175	28	0.063	28	0.064
0.53	0.4	0.371	1778	19.7	0.226	0.177	28	0.065		
0.53	0.8	0.371	1784	20.5	0.224	0.174	24	0.055	26	0.057
0.53	0.8	0.371	1784	20.5	0.225	0.175	26	0.059		
0.63	0.4	0.332	1642	19.7	0.225	0.175	19	0.039	19	0.039
0.63	0.4	0.332	1642	19.7	0.225	0.175	19	0.040		
0.63	0.8	0.332	1706	20.2	0.224	0.174	19	0.041	19	0.041

Table 7: Parameters measured with the Marsh funnel for paste made with 75% CEM I 52.5-SR + 25% GGBS. Volume introduced, 0.8 dm^3; drained volume, 0.4 dm^3.

w/c	*SP*/c	ϕ_c	ρ_p [kg/m^3]	T [°C]	H_0 [m]	H [m]	t_f [s]	η_p [Pa s]	$t_{f,\mathrm{av}}$ [s]	$\eta_{p,\mathrm{av}}$ [Pa s]
0.35	0.4	0.487	1989	21.0	0.226	0.177	99	0.258	104	0.268
0.35	0.4	0.487	1989	21.0	0.227	0.179	107	0.279		
0.35	0.8	0.487	2001	20.6	0.226	0.177	73	0.189	73	0.189
0.35	0.8	0.487	2001	20.6	0.226	0.177	72	0.188		
0.47	0.4	0.414	1814	20.9	0.225	0.175	28	0.065	28	0.066
0.47	0.4	0.414	1814	20.9	0.225	0.175	28	0.066		
0.47	0.8	0.414	1864	20.3	0.223	0.172	27	0.066	28	0.067
0.47	0.8	0.414	1864	20.3	0.225	0.175	28	0.069		
0.63	0.4	0.345	1713	18.1	0.225	0.175	18	0.040	20	0.042
0.63	0.4	0.345	1713	18.1	0.226	0.177	20	0.045		
0.63	0.8	0.345	1602	20.5	0.221	0.169	19	0.038	19	0.038
0.63	0.8	0.345	1602	20.5	0.220	0.167	19	0.038		

Table 8: Parameters measured with the Marsh funnel for paste made with CEM II 32.5 BL–II. Volume introduced, 0.8 dm^3; drained volume, 0.4 dm^3.

w/c	*SP*/c	ϕ_c	ρ_p [kg/m^3]	T [°C]	H_0 [m]	H [m]	t_f [s]	η_p [Pa s]	$t_{f,\mathrm{av}}$ [s]	$\eta_{p,\mathrm{av}}$ [Pa s]
0.35	0.4	0.476	1967	20.1	0.226	0.177	96	0.246	98	0.250
0.35	0.4	0.476	1967	20.1	0.226	0.177	99	0.253		
0.35	0.8	0.476	1989	20.3	0.225	0.175	77	0.199	78	0.201
0.35	0.8	0.476	1989	20.3	0.224	0.174	79	0.203		
0.47	0.4	0.405	1820	19.2	0.224	0.174	40	0.093	38	0.087
0.47	0.4	0.405	1820	19.2	0.225	0.175	35	0.082		
0.47	0.8	0.405	1818	20.0	0.223	0.172	26	0.060	30	0.070
0.47	0.8	0.405	1818	20.0	0.226	0.177	34	0.079		
0.53	0.4	0.377	1771	19.5	0.226	0.177	31	0.072	31	0.071
0.53	0.4	0.377	1771	19.5	0.225	0.175	30	0.069		
0.53	0.8	0.377	1741	19.7	0.225	0.175	30	0.066	26	0.057
0.53	0.8	0.377	1741	19.7	0.225	0.175	22	0.048		
0.63	0.4	0.338	1725	17.9	0.225	0.175	18	0.041	18	0.041
0.63	0.4	0.338	1725	17.9	0.226	0.177	18	0.041		
0.63	0.8	0.338	1695	19.5	0.217	0.162	21	0.042	20	0.041
0.63	0.8	0.338	1695	19.5	0.218	0.164	19	0.040		

Table 9: Parameters measured with the Marsh funnel for paste made with 75% CEM II 32.5 BL–II + 25% GGBS. Volume introduced, 0.8 dm^3; drained volume, 0.4 dm^3.

w/c	*SP*/c	ϕ_c	ρ_p [kg/m^3]	T [°C]	k_1 [mm^2 s^2]	k_2 [mm^2 s^2]	t_1 [s]	t_2 [s]	η_p [Pa s]
0.35	0.4	0.477	2017	21.0	1.10491	0.84138	79	148	0.214
0.35	0.8	0.477	2025	23.4	1.10508	0.84151	53	68	0.117
0.47	0.4	0.404	1868	23.2	1.10507	0.84150	43	54	0.087
0.47	0.8	0.404	1828	21.0	1.10491	0.84138	21	20	0.037
0.53	0.4	0.376	1776	23.6	1.10510	0.84153	22	26	0.042
0.53	0.8	0.376	1772	21.0	1.10491	0.84138	12	14	0.022
0.63	0.4	0.336	1602	20.0	1.10483	0.84133	11	24	0.027
0.63	0.8	0.336	1743	20.6	1.10488	0.84136	7	7	0.012

Table 10: Parameters measured with the Cannon–Fenske viscometer (400 series) on paste CEM I 52.5–SR

w/c	*SP*/c	ϕ_c	ρ_p [kg/m^3]	T [°C]	k_1 [mm^2 s^2]	k_2 [mm^2 s^2]	t_1 [s]	t_2 [s]	η_p [Pa s]
0.35	0.4	0.471	1993	22.2	1.10499	0.84145	51	121	0.158
0.35	0.8	0.471	1997	22.8	1.10504	0.84148	50	114	0.151
0.47	0.4	0.399	1854	21.2	1.10492	0.84139	21	47	0.058
0.47	0.8	0.399	1844	22.0	1.10498	0.84144	17	20	0.033
0.53	0.4	0.371	1778	21.0	1.10491	0.84138	16	34	0.041
0.53	0.8	0.371	1784	22.1	1.10499	0.84144	14	16	0.026
0.63	0.4	0.332	1642	20.4	1.10486	0.84135	9	11	0.016
0.63	0.8	0.332	1743	21.2	1.10492	0.84139	9	10	0.016

Table 11: Parameters measured with the Cannon–Fenske viscometer (400 series) on paste 75% CEM I 52.5–SR + 25% GGBS

w/c	*SP*/c	ϕ_c	ρ_p [kg/m^3]	T [°C]	k_1 [mm^2 s^2]	k_2 [mm^2 s^2]	t_1 [s]	t_2 [s]	η_p [Pa s]
0.35	0.4	0.487	1989	26.8	1.10533	0.84170	48	73	0.114
0.35	0.8	0.487	2001	22.0	1.10498	0.84144	34	42	0.073
0.47	0.4	0.414	1814	21.4	1.10494	0.84140	15	19	0.030
0.47	0.8	0.414	1864	20.8	1.10489	0.84137	16	16	0.029
0.63	0.4	0.345	1713	19.8	1.10482	0.84132	8	17	0.020
0.63	0.8	0.345	1602	20.0	1.10483	0.84133	8	9	0.013

Table 12: Parameters measured with the Cannon–Fenske viscometer (400 series) on paste 100% CEM II 32.5 BL–II

w/c	*SP*/c	ϕ_c	ρ_p [kg/m^3]	T [°C]	k_1 [mm^2 s^2]	k_2 [mm^2 s^2]	t_1 [s]	t_2 [s]	η_p [Pa s]
0.35	0.4	0.476	1967	20.8	1.10489	0.84137	42	50	0.087
0.35	0.8	0.476	1989	21.4	1.10494	0.84140	34	44	0.074
0.47	0.4	0.405	1820	20.0	1.10483	0.84133	19	22	0.036
0.47	0.8	0.405	1818	21.0	1.10491	0.84138	14	18	0.028
0.53	0.4	0.377	1771	18.8	1.10475	0.84126	14	16	0.026
0.53	0.8	0.377	1741	20.4	1.10486	0.84135	11	14	0.021
0.63	0.4	0.338	1725	19.4	1.10479	0.84129	9	19	0.022
0.63	0.8	0.338	1695	20.8	1.10489	0.84137	6	8	0.011

Table 13: Parameters measured with the Cannon–Fenske viscometer (400 series) on paste 75% CEM II 32.5 BL–II + 25% GGBS

Admixture	w/c	SP/c	ϕ_c	ρ_p [kg/m^3]	T [°C]	H_0 [m]	H [m]	t_d [s]
Polycarboxylate	0.35	0.4	0.477	2058	20.8	0.224	0.184	116
	0.35	0.8	0.477	2054	20.8	0.224	0.178	100
	0.47	0.4	0.404	1878	21.1	0.224	0.180	34
	0.47	0.8	0.404	1838	21.1	0.224	0.179	34
	0.53	0.4	0.376	1802	21.0	0.234	0.194	22
	0.53	0.8	0.376	1813	21.0	0.225	0.178	23
	0.63	0.4	0.336	1696	21.0	0.222	0.172	18
	0.63	0.8	0.336	1706	21.0	0.224	0.181	17
Poly–aryl–ether	0.40	1.0	0.443	1934	22.0	0.224	0.164	65
	0.40	1.2	0.443	1962	22.0	0.228	0.187	35
	0.47	1.0	0.404	1856	21.1	0.224	0.179	35
	0.47	1.2	0.404	1842	21.0	0.222	0.173	31
	0.53	1.0	0.376	1816	22.0	0.224	0.179	24
	0.53	1.2	0.376	1821	22.0	0.227	0.183	20
	0.63	1.0	0.336	1728	22.0	0.226	0.181	17
	0.63	1.2	0.336	1728	22.0	0.225	0.180	17

Table 14: Parameters measured using the Marsh funnel in CEM I 52.5–SR cement pastes with two types of superplasticizer admixture. Volume introduced, 0.8 dm^3; drained volume, 0.4 dm^3.